

INDIAN INSTITUTE OF SCIENCE
BANGALORE – 560 012
INDIA

FINAL TECHNICAL REPORT

ELECTROCHEMICAL INVESTIGATIONS OF THE
INTERFACE AT Li/Li^+ ION CONDUCTING CHANNEL



PRINCIPAL INVESTIGATOR

PROF. MUNICHANDRAIAH NOOKALA
DEPARTMENT OF INORGANIC AND PHYSICAL CHEMISTRY

SUBMITTED TO

ASIAN OFFICE OF AIR FORCE RESEARCH AND DEVELOPMENT
7-23-17 ROPPONGI, MINATO-KU, TOKYO 106-0032, JAPAN

Report Documentation Page			Form Approved OMB No. 0704-0188		
Public reporting burden for the collection of information is estimated to average 1 hour per response, including the time for reviewing instructions, searching existing data sources, gathering and maintaining the data needed, and completing and reviewing the collection of information. Send comments regarding this burden estimate or any other aspect of this collection of information, including suggestions for reducing this burden, to Washington Headquarters Services, Directorate for Information Operations and Reports, 1215 Jefferson Davis Highway, Suite 1204, Arlington VA 22202-4302. Respondents should be aware that notwithstanding any other provision of law, no person shall be subject to a penalty for failing to comply with a collection of information if it does not display a currently valid OMB control number.					
1. REPORT DATE 04 OCT 2006		2. REPORT TYPE Final Report (Technical)		3. DATES COVERED 01-03-2004 to 01-10-2006	
4. TITLE AND SUBTITLE Electrochemical Investigations of the Interface at Li/Li+ Ion Conducting Channel				5a. CONTRACT NUMBER	
				5b. GRANT NUMBER	
				5c. PROGRAM ELEMENT NUMBER	
6. AUTHOR(S) Munichandraiah Nookala				5d. PROJECT NUMBER	
				5e. TASK NUMBER	
				5f. WORK UNIT NUMBER	
7. PERFORMING ORGANIZATION NAME(S) AND ADDRESS(ES) Indian Institute of Science, Department of Inorganic and Physical Chemistry, Bangalore 560 012, INDIA, IN, 560012				8. PERFORMING ORGANIZATION REPORT NUMBER AOARD-044030	
9. SPONSORING/MONITORING AGENCY NAME(S) AND ADDRESS(ES) The US Research Laboratory, AOARD/AFOSR, Unit 45002, APO, AP, 96337-5002				10. SPONSOR/MONITOR'S ACRONYM(S) AOARD/AFOSR	
				11. SPONSOR/MONITOR'S REPORT NUMBER(S)	
12. DISTRIBUTION/AVAILABILITY STATEMENT Approved for public release; distribution unlimited					
13. SUPPLEMENTARY NOTES					
14. ABSTRACT Dilithium phthalocyanine (Li2Pc) possesses mixed electronic-ionic conductivity due to overlap of orbitals (electronic) and mobility of Li+ ion (ionic) in a channel formed due to stacking of the macromolecules. Electrochemical impedance measurements provide separation of electronic and ionic conductivities. The temperature dependence studies are employed for calculation of activation energies. The electronic conductivity shows a marked increase on applying DC bias voltage across a symmetrical cell of Li2Pc with blocking electrodes, whereas the ionic conductivity is marginally influenced.					
15. SUBJECT TERMS Batteries, Electrochemistry, Propulsion					
16. SECURITY CLASSIFICATION OF:			17. LIMITATION OF ABSTRACT	18. NUMBER OF PAGES 77	19a. NAME OF RESPONSIBLE PERSON
a. REPORT unclassified	b. ABSTRACT unclassified	c. THIS PAGE unclassified			

CONTENTS

1. Analysis of electrochemical impedance of dilithium phthalocyanine	3
2. Electrodeposition of adherent films of lithium phthalocyanine on platinum and stainless steel substrates by oxidation of dilithium phthalocyanine	16
3. Studies on composite of dilithium phthalocyanine and iodine	40
4. Thin film of dilithium phthalocyanine impregnated Celgrad membrane	47
5. Impedance of dilithium phthalocyanine in contact with different metallic substrates	50
6. Capacitor studies of dilithium phthalocyanine and lithium Phthalocyanine	56
7. Dilithium phthalocyanine as a cathode material	63
8. List of publications	76
9. Acknowledgements	77

1. Analysis of electrochemical impedance of dilithium phthalocyanine

Abstract

Dilithium phthalocyanine (Li_2Pc) possesses mixed electronic-ionic conductivity due to overlap of π - π orbitals (electronic) and mobility of Li^+ ion (ionic) in a channel formed due to stacking of the macromolecules. Electrochemical impedance measurements provide separation of electronic and ionic conductivities. The temperature dependence studies are employed for calculation of activation energies. The electronic conductivity shows a marked increase on applying DC bias voltage across a symmetrical cell of Li_2Pc with blocking electrodes, whereas the ionic conductivity is marginally influenced.

Introduction

The phthalocyanine (Pc) is a centro symmetric planar molecule with the general formula $\text{C}_{32}\text{H}_{18}\text{N}_8$ and it does not contain any polar group. Metal phthalocyanines (MPc) have been under extensive investigations because of their potential use in a wide range of applications.¹ Presently, these molecules are of particular interest in non-linear optics, as liquid crystals, as Langmuir-Blodgett films, for fabrication of self assembled monolayers, in optical data storage, as electrochromic substances, as gas sensors, as semiconductors, in electrocatalysis, as photosensitizers and as photoconductors. The interesting properties of these compounds are due to the conjugated electronic structure of the macro cycle and also to the presence of metal ion, which is usually divalent, at the center of the molecule.² It has been known that the MPc molecules are stacked in an array in different ways resulting in α , β and χ forms of crystallographic structures.³ In these closely arranged structures, there is a considerable overlap of π - π orbitals among adjacent MPc molecules, which results in the formation of one dimensional electronic conduction path.⁴ The electronic conductivity varies over a wide range, and depends on the method of preparation and other experimental conditions; but these compounds are generally considered as semiconductors. The potentially useful properties of MPc include optical, electronic as well as electrochemical. These compounds have been studied as cathode

materials in rechargeable batteries.^{5,6} Several metal phthalocyanines have been investigated for their catalytic activity on carbon cathodes of Li/SOCl₂ cells.⁷

Dilithium phthalocyanine (Li₂Pc) is different from MPc with respect to the number of metal atoms per phthalocyanine molecule and also with respect to the position of the metal atom. In the case of divalent M, it is located at the center of the Pc producing a planar MPc molecule. On the other hand, the two Li atoms in Li₂Pc are positioned on either side of the Pc macrocycle and the distance between the two Li atoms has been estimated as 1.99 Å.⁸ There has been interest in investigating the mobility of Li⁺ ion in the array of Li₂Pc molecules.⁹ It has been found that the intramolecular distance between two lithium atoms increases from 1.99 Å for a single Li₂Pc molecule to a value as large as 2.67 Å for self assembled structures.⁸ The increase in the Li-Li distance may be a reflection of the weakening of Li-N bond which would facilitate the mobility of the Li⁺ ions in the self assembled structure. Thus in addition to the electronic conductivity, the ionic conduction occurs due to the mobility of single ionic species in a channel formed due to stacking of Li₂Pc macromolecules. The Li⁺ ion conducting property has been utilized to study a solid-state Li/LiMnO₂ cell employing Li₂Pc as the solid electrolyte.¹⁰ Thus there are two modes of charge transport – electronic and ionic in Li₂Pc. There are no experimental studies reported to clearly establish these two modes of conductivity in Li₂Pc using AC impedance studies. The AC impedance is a versatile technique to characterize the interfacial as well as bulk properties of an electrochemical system by conducting the measurements over a wide frequency range and at various potentials.

The aim of the present study is to investigate the AC impedance properties of Li₂Pc. The impedance data are analyzed using an appropriate equivalent circuit and non-linear least squares (NLLS) fitting procedure for obtaining the ionic and electronic conductivities. The results suggest that the ionic conductivity of Li₂Pc is greater than the electronic conductivity by an order of magnitude. The effects of temperature and DC bias voltage are also investigated.

Experimental

The Li₂Pc was purchased from Aldrich and recrystallized from acetone and toluene. Pellets of 10 mm diameter and about 250 μm thick were made by pressing at 32 kN cm⁻² a mixture of Li₂Pc powder (85 wt%) and polyvinylidene fluoride (15 wt%) as

the binder. Before pressing, the mixture was subjected to copious grinding using plexiballs in a Wig-L-Bug grinder/mixer. The pellets were transferred to a argon filled glove box (MBraun model UNILab) with moisture and oxygen impurities less than 10 ppm. Symmetrical cells - SS/Li₂Pc/SS, where SS refers to stainless steel, were assembled in home-made Teflon holders. The cells were inserted into air-tight glass containers having provision to take electrical leads. The cells were heated to the required temperature by means of an electrical heating coil surrounding the glass container, and a temperature controller. The temperature was maintained with an accuracy of ± 1 °C. AC impedance of the cells in the frequency range from 100 kHz to 10 mHz with an excitation signal of 50 mV was measured using EG&G PARC Impedance Analyzer model 6310 and the NLLS analysis of the data was carried out using the software program Z Plot of Scribner Associates, which was supplied by Solartron. The impedance data were measured at several temperatures between the ambient and 80 °C and also by applying different DC bias voltages across the cell.

Results and discussion.

A typical Nyquist diagram of AC impedance data of SS/Li₂Pc/SS cell is shown in Fig. 1. The diagram consists of a pair of semicircles suggesting the presence of two relaxation processes. In view of the electronic and ionic conduction paths, which are independent of each other, the electronic resistance (R_e) and the ionic resistance (R_i) are considered in parallel in an equivalent circuit. Accordingly, the appropriate equivalent circuit is shown in Fig. 2. The interfacial capacitance (C_{int}) due to the interface between SS and Li₂Pc is considered in series with R_i and the geometric capacitance (C_g) is in parallel to the rest of circuit elements (Fig. 2(a)). A similar equivalent circuit has been employed for measuring transference numbers of some perovskite-like oxides.¹¹ For the purpose of obtaining the values of these impedance parameters, the data are analyzed as follows:

The low frequency intercept, R_2 (Fig. 1) is equivalent to the DC resistance. Considering that the capacitances C_g and C_{int} block, and only the resistance R_2 allows the DC flow in the circuit (Fig. 2(a)), it is obvious that $R_2 = R_e$. Thus R_e can be obtained from low frequency intercept of the Nyquist impedance diagram (Fig. 1). The capacitive reactance (X) is defined as,

$$X = 1 / (2 \pi f C) \quad (1)$$

where, f is frequency and C is capacitance. It is generally known¹¹ that the $C_g < C_{int}$, and therefore, $X_g > X_{int}$, where X_g and X_{int} are reactances due to geometric capacitance and interfacial capacitance, respectively. At high frequencies, $X_{int} < R_i$, and therefore the equivalent circuit can be approximated to the one shown in Fig. 2(b). Thus, the high frequency semicircle is due to the parallel combination of R_e , R_i and C_g . The diameter, or intercept of high frequency semicircle (R_1) shown in Fig. 1 is equal to the parallel combination of electronic resistance (R_e) and ionic resistance (R_i) of the Li_2Pc pellet. The value of R_i can be estimated as,

$$R_i = R_e R_1 / (R_e - R_1) \quad (2)$$

The geometric capacitance (C_g) may be calculated from the frequency (f^*) corresponding to the maximum of the high frequency semicircle as,

$$C_g = 1 / (2 \pi f^* R_1) \quad (3)$$

At low frequencies, $X_g > (X_{int} + R_e)$, and therefore the equivalent circuit can be approximated to as the one shown in Fig. 2(c). The diameter of the low frequency semicircle corresponds to the resistance equivalent to $(R_e - R_1)$. The value of C_{int} can be obtained from Eq. 4.

$$C_{int} = 1 / (2 \pi f^{**} (R_e - R_1)) \quad (4)$$

where, f^{**} is frequency corresponding to the maximum of low frequency semicircle.

Thus the values of R_i , R_e , C_g and C_{int} can be obtained from the pair of semicircles (Fig. 1). For the purpose of evaluating these resistances using a NLLS fitting program, the equivalent circuit (Fig. 2(a)) is modified by replacing the capacitance with constant phase elements (CPE), Q . The need of employing CPE arises due to the fact that the semicircles (Fig. 1) are distorted and their origins lie below the real axis (Fig. 1).¹² This is due to heterogeneous nature of the interfaces in microscopic scale. A CPE is defined as:¹³

$$Q = Q_0 j^{\omega n} \quad (5)$$

where, Q_0 is an adjustable parameter, $\omega = 2\pi f$, f is the frequency and n is a constant. For $n = 0$, CPE represents a resistance, $R (= Q_0^{-1})$; for $n = 1$, a capacitance, $C (= Q_0)$; for $n = 0.5$, a Warburg impedance; and for $n = -1$, an inductance, $L (= Q_0^{-1})$.

Approximate values of the circuit elements were obtained from the experimental data and the NLLS fitting program was initialized. After several iterations, the best fit

parameters were obtained. The theoretical impedance curve generated from the fit values is shown in Fig. 1 as the solid line and the values are given in the caption. It is seen that there is a good agreement between the experimental data and the theoretical curve. The values of errors are less than 5 % for all impedance parameters, except 14 % for CPE_g . Furthermore, the value of χ^2 is less than 1×10^{-3} suggesting a high confidence level in fitting the data. The values of n_{int} and n_g are close to unity, and therefore the constant phase elements are considered equal to the corresponding capacitances. It may be noted that C_g is about 5.97×10^{-11} F, which is less than 4.54×10^{-9} F for C_{int} , supporting the assumption made previously.

Using the values of R_i and R_e , the respective specific conductivity (σ) values were calculated.

$$\sigma = l / (A R) \quad (6)$$

where, R represents either R_i or R_e , l is thickness of Li_2Pc pellet and A is area of SS electrode. From the data shown in Fig. 1, the values of σ_i and σ_e obtained are 1.56×10^{-7} and $1.29 \times 10^{-8} \text{ S cm}^{-1}$, respectively. It is interesting to note that σ_i is higher than σ_e by an order of magnitude.

Zhang et al.⁸ have employed molecular dynamics simulations to investigate structural and dynamical properties of self assembly of Li_2Pc . To investigate the mobility of Li^+ ion, the velocity correlation function, which is related to self diffusion coefficient (D), has been calculated. The velocity correlation function of Li^+ has been shown to oscillate in the time domain, indicating rattling motion of Li^+ ions in the cage of their nearest neighbor. The corresponding conductivity (σ_i) of Li^+ ions has been calculated using the Nernst-Einstein equation. The values of σ_i vary in the range of 2.65×10^{-5} - $8.40 \times 10^{-5} \text{ S cm}^{-1}$ at 27°C , the variation being dependent on the crystalline forms of Li_2Pc . The σ_i value obtained in the present study is less than these theoretically calculated values by about one to two orders of magnitude. Among the metal phthalocyanines, the ionic conducting feature appears to be unique for Li_2Pc . In the present study, the electronic conductivity is obtained in addition to the ionic conductivity.

Investigations on solid polymer electrolytes (SPEs) have been intense in recent years because of their potential use in solid state rechargeable lithium batteries.¹⁴ Existence of ionic transport in a complex of poly(ethyleneoxide), PEO, and a lithium salt

has been the origin of these studies. The specific ionic conductivity of these SPEs is about $1 \times 10^{-8} \text{ S cm}^{-1}$ at ambient temperature. It may be noted that the ionic conductivity obtained for Li_2Pc is at least an order of magnitude higher in comparison with PEO based SPEs. Additionally, the ionic conduction in Li_2Pc occurs due to the mobility of Li^+ ion alone, whereas it is due to both Li^+ ion and the anion in SPEs.

The temperature dependence of conductivity of PEO based SPEs has been of great importance.¹⁴ The specific conductivity increases from $1 \times 10^{-8} \text{ S cm}^{-1}$ at ambient temperature to about $1 \times 10^{-4} \text{ S cm}^{-1}$ at 80°C , thus showing a strong dependence on temperature. The temperature dependence has been found to be Arrhenius (Eq. 7) as well as non-Arrhenius relationships in different cases.

$$\sigma_i = A \exp(-E_a / (R T)) \quad (7)$$

where, A is a constant and E_a is activation energy. For instance, in the case of the SPE made of the PEO and LiClO_4 , a plot of σ_i versus $1/T$ had two linear segments with a transition at 70°C , which is the melting point (T_m) of PEO complex. Thus the conduction followed Arrhenius behavior in temperature regions both below and above T_m . In the case of the SPE made of PEO and NaSCN , the conduction followed Arrhenius behavior below the T_m and non-Arrhenius behavior above T_m . In the case of SPE made of PEO and CsSCN , however, the ionic conduction showed non-Arrhenius behavior throughout the temperature range ($20 - 120^\circ\text{C}$). In the present study, both σ_i and σ_e of Li_2Pc are found to follow Arrhenius relationship with temperature (Fig. 3), and the activation energies obtained for ionic and electronic conduction processes are, respectively, 0.20 and 0.24 eV. There is an increase in σ_i and σ_e with increase of temperature. The increase in σ_i , however, is not high unlike in the case of PEO based SPEs.

The impedance spectra of a $\text{SS}/\text{Li}_2\text{Pc}/\text{SS}$ symmetrical cell were recorded at several DC voltages applied across the cell. A set of Nyquist plots is shown in Fig. 4. It is seen that the high frequency semicircle remains nearly unaltered at all DC bias voltages. However, there is a substantial decrease in low frequency semicircle with an increase of DC bias voltage. Whereas σ_i calculated at several voltages is nearly constant at a given temperature, σ_e increases with an increase of DC bias voltage as shown in Fig. 5. The increase in σ_e is likely to be due to greater overlap of π - π orbitals. Similar to the present results, capacitor properties of other metallophthalocyanines show a strong dependence

on the DC voltage.¹⁵ The values of activation energy for σ_i and σ_e at different DC bias voltages are nearly the same as those obtained at open circuit.

There has been interest in developing solid electrolytes using PEO-type polymers for solid-state lithium batteries. Although the intrinsic Li^+ ion conductivity of Li_2Pc is greater than its electronic conductivity and also in comparison with ionic conductivity of PEO-based SPEs, the magnitude of electronic conductivity as well as its marked dependence on voltage are rather undesirable for practical applications as an electrolyte. For this purpose, σ_e probably should be $< 1 \times 10^{-10} \text{ S cm}^{-1}$ against the present value of $1.29 \times 10^{-8} \text{ S cm}^{-1}$ at ambient temperature. Investigations leading to appropriate experimental conditions, which provide higher σ_i and lower σ_e are underway.

Conclusions

Unlike most metallophthalocyanines, which are one dimensional semiconductors due to electron transfer, Li_2Pc possesses both electronic and ionic conducting paths. The AC impedance spectra of Li_2Pc pellets are measured at different temperatures and several DC bias voltages. The Nyquist impedance data reflect the presence of two relaxation processes. The data are analyzed with the aid of an appropriate equivalent circuit and non-linear least squares fitting program. It is noteworthy that the ionic conductivity is higher than the electronic conductivity at ambient temperature and open circuit of the symmetrical cells. The electronic conductivity increases with DC bias voltage due to increasing overlap of π - π orbitals.

References

1. M. Hanack and L.R. Subramanian, *Handbook of Organic Conductive Molecules and Polymers* Vol. 1, H.S. Nalwa, Editor, John Wiley & Sons (1997) p. 687.
2. H. Schultz, H. Lehmann, M. Rein, and M. Hanack, *Structure and Bonding*, **74**, 41 (1991).
3. R.D. Gould, *Coord. Chem. Rev.*, **156**, 237 (1996).
4. S. Venkatachalam, *Handbook of Organic Conductive Molecules and Polymers* Vol. 2, H.S. Nalwa, Editor, John Wiley & Sons (1997) p. 741.
5. J.I. Yamaki and A. Yamaji, *J. Electrochem. Soc.*, **129**, 5 (1982).

6. S. Okada and J.I. Yamaki, *J. Electrochem. Soc.*, **136**, 2437 (1989).
7. K.M. Abraham, M. Alamgir, E.B. Willstaedt and W.P. Kilroy, *Electrochim. Acta*, **37**, 531 (1992).
8. Y. Zhang, P. R. Alonso, A. Martinez-Limia, L. G. Scanlon and P.B. Balbuena, *J. Phys. Chem. B*, **108**, 4659 (2004).
9. L.G. Scanlon, L.R. Lucente, W.A. Feld, G. Sandi, D. Campo, A. Turner, C. Johnson, and R. Marsh, in *Proceedings of the International Workshop on Electrochemical Systems*, A. R. Landgrebe and R. J. Klingler, Editors, **36**, 326 (2000).
10. L.G. Scanlon, L.R. Lucente, W.A. Feld, G. Sandi, P.B. Balbuena, P.R. Alonso, and A. Turner, *J. Electrochem. Soc.*, **151**, A1338 (2004).
11. V. Thangadurai, R. A. Huggins and W. Weppner, *J. Power Sources*, **108**, 64 (2002).
12. J.R. Macdonald, *Impedance Spectroscopy*, John Wiley & Sons, New York (1987) p. 1.
13. B.A. Boukamp, *Equivalent Circuit, Users Manual*, University of Twente, The Netherlands (1989) p. 1.
14. M.B. Armand, J.R. MacCallum, C.A. Vincent, *Polymer Electrolyte Reviews*, Vol. 1, Elsevier Applied Science, London (1987) p.1.
15. R.W. Esfahani and G.J. Maclay, *J. Appl. Phys.*, **67**, 3409 (1990).

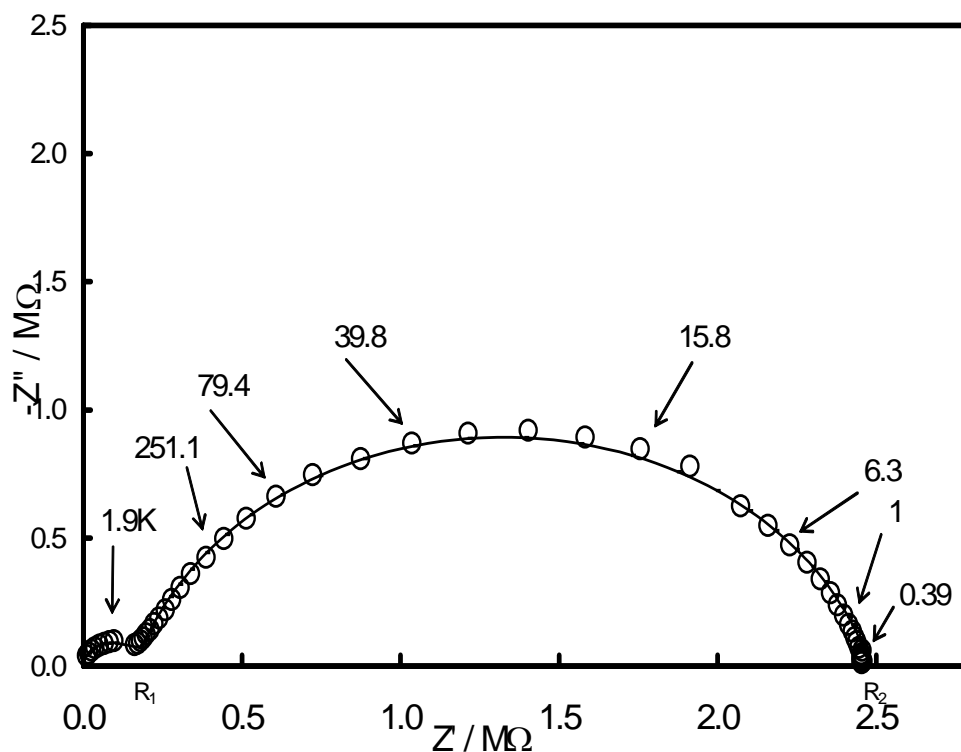


Figure 1. AC impedance spectrum of a SS/Li₂Pc/SS symmetrical cell at 25°C. The experimental data are shown as circles and the theoretical data obtained from NLLS fit as the solid curve. The frequency values (in Hz) are shown for some of the data points. The values of impedance parameters obtained from the NLLS analysis are as follows: $R_e = 2.47 \times 10^6$, $R_i = 2.09 \times 10^5$, $CPE_{int} = 4.54 \times 10^{-9}$, $n_{int} = 0.85$, $CPE_g = 5.97 \times 10^{-11}$ and $n_g = 0.98$.

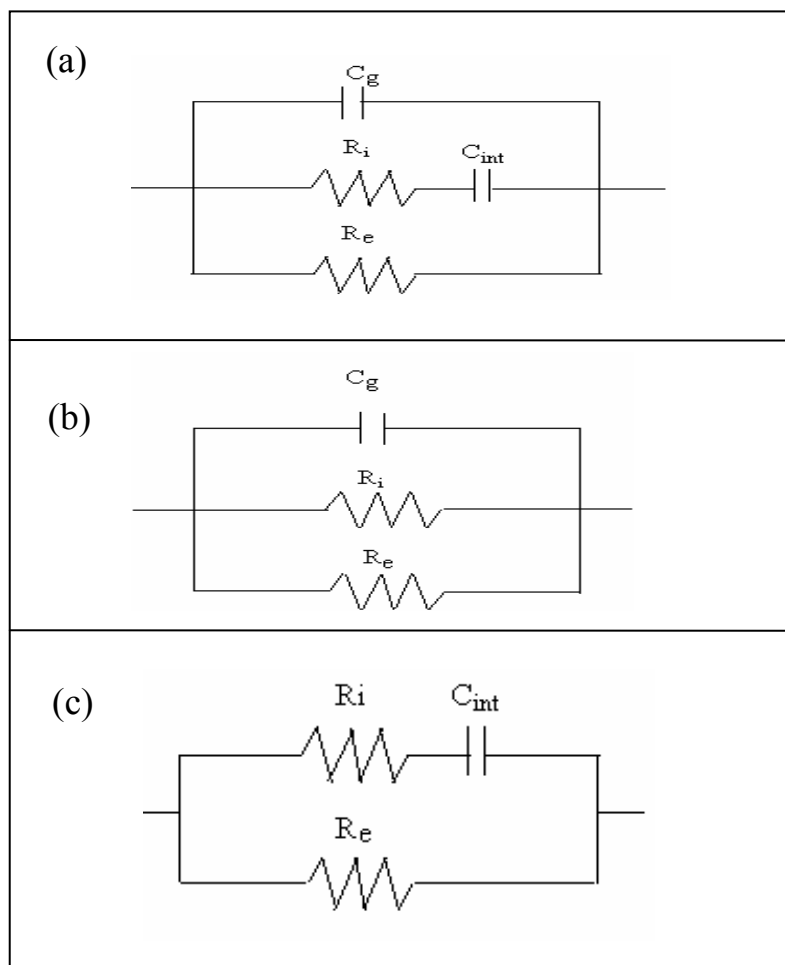


Figure 2. Equivalent circuits covering (a) the whole frequency range, (b) approximated to the high frequency range and (c) approximated to the low frequency range. See text for symbols.

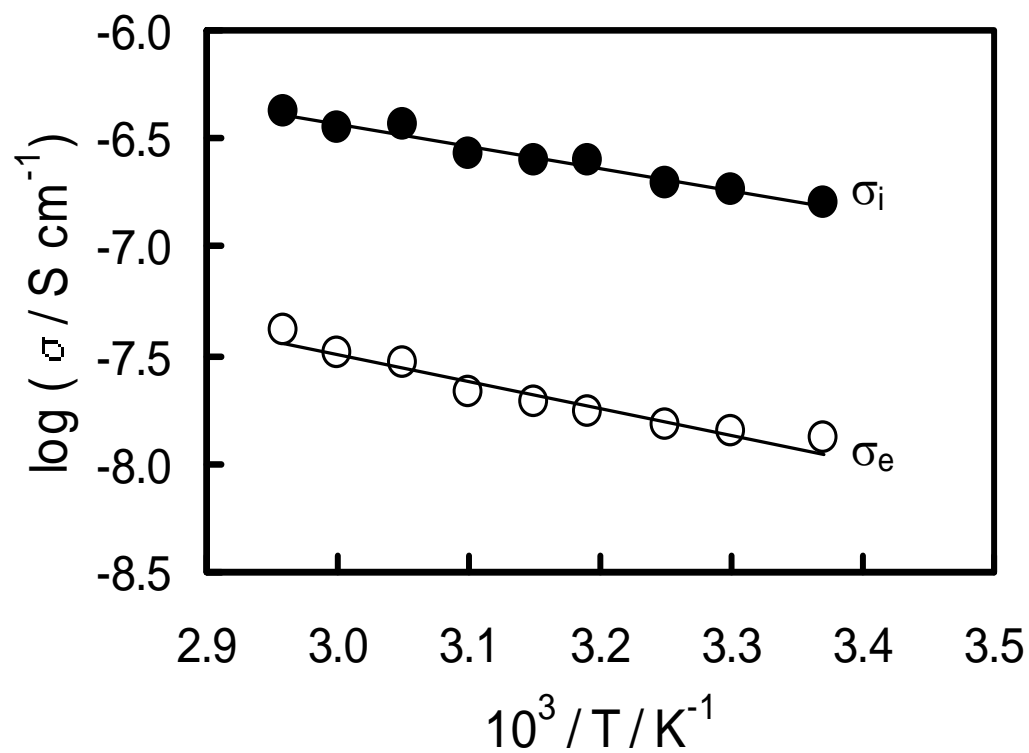


Figure 3. Arrhenius plots of (a) electronic conductivity and (b) ionic conductivity at open circuit.

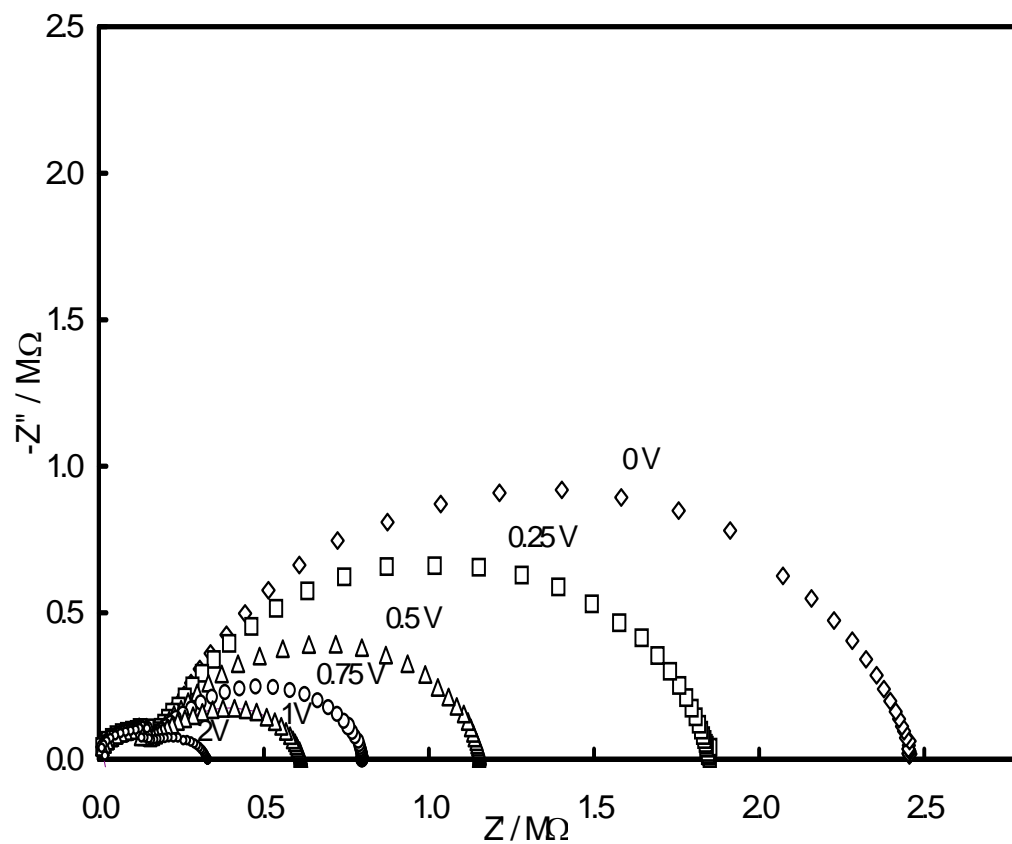


Figure 4. Nyquist diagrams of SS/Li₂Pc/SS cell at 25 °C measured at several DC bias voltages indicated at each diagrams.

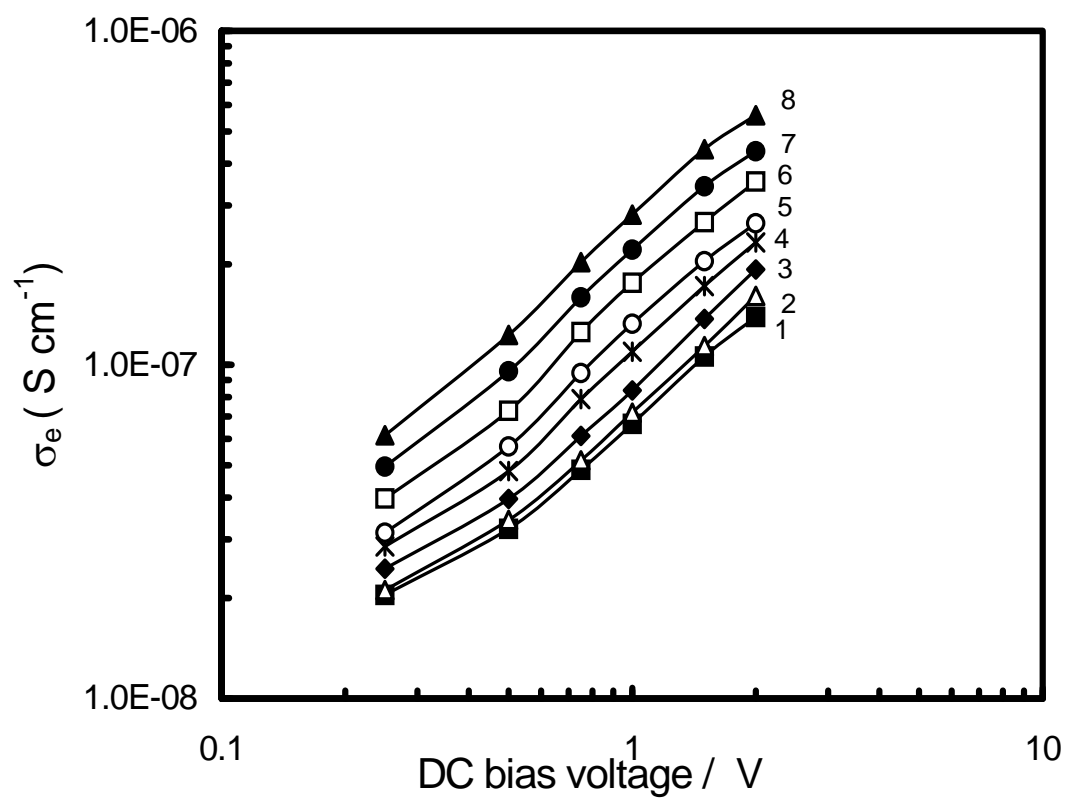


Figure 5. Variation of specific electronic conductivity (σ_e) with DC bias voltage at 30 (1), 35 (2), 40 (3), 45 (4), 50 (5), 55 (6), 60 (7) and 65 °C (8).

2. Electrodeposition of adherent films of lithium phthalocyanine on platinum and stainless steel substrates by oxidation of dilithium phthalocyanine

Abstract

Films of lithium phthalocyanine (LiPc) on Pt and stainless steel (SS) substrates are deposited by electrochemical oxidation of dilithium phthalocyanine (Li_2Pc) in dimethyl sulphoxide or acetone consisting of LiBF_4 as the supporting electrolyte. Unlike the powdery deposits of LiPc obtained by using tetrabutyl ammonium perchlorate (TBAP) as the supporting electrolyte, the deposits are adherent to the substrates when LiBF_4 is used as the supporting electrolyte. Chemical oxidation of Li_2Pc by TBAP is shown to be detrimental for the formation of powdery electrodeposits of LiPc, whereas LiBF_4 does not oxidize Li_2Pc and therefore adherent films of LiPc are obtained by electrooxidation. Furthermore, the kinetics of electrooxidation of Li_2Pc to LiPc appear to be different in TBAP and LiBF_4 solutions as inferred from the nature of cyclic voltammograms and also the values of transfer coefficient. The oxidation of Li_2Pc occurs at higher potentials on SS in relation to the reaction on Pt. Nevertheless, LiPc films are adherent on both substrates. The LiPc/Pt electrodes exhibit electrochemical activity, whereas LiPc/SS electrodes exhibit capacitive behaviour. The texture of LiPc on both Pt and SS is found to be fibres-like.

Introduction

Molecular organic semiconductors and molecular metals find increasing importance in recent years due to their tunable electrical and chemical properties, and also various applications.¹⁻³ Applications of these materials include rectifiers, field effect transistors, electromagnetic shielding, video disk coatings, light emitting diodes, photoresists, photovoltaics, electrochromics, batteries, fuel cells and sensors.^{1,2} Metal phthalocyanines and their derivatives in partially oxidized state and also with dopants behave as molecular metals.²⁻⁵ Lithium phthalocyanine radical (LiPc), which is reported as a stable monophthalocyanine radical with low band gap intrinsic semiconductority, is used as an oxygen probe in biological systems and also in magnetometry.⁶⁻⁸ The π electron cloud of LiPc is delocalized in the macrocycle and also throughout the intermolecular stacking. Phthalocyanines have been known to exhibit polymorphism and hence the crystal structure greatly affects the electronic properties of these materials.

LiPc exists in χ , α and β forms.⁹ The tetragonal χ form has low band gap due to effective intermolecular stacking. The magnetic properties vary with spin delocalization and intermolecular stacking of different forms. Diffusion of the gas molecules (O_2 , NO) through the crystallographic channels (0.6 nm) is effective in the χ form.^{8,10} No charge transfer takes place between O_2 and LiPc radical, and the conductivity is not modified. Due to the nearest-neighbour distance LiPc-LiPc which is considerably shorter than the Van der Waals distance, the spin dynamics are unusual and very narrow EPR lines are observed. The strong π overlaps within the stacks enable strong interactions which result in broad electronic bands and an energy gap of 0.2 eV, characterizing the semiconducting properties in a wide temperature range. The main characteristics of the radicals for the EPR magnetometry are the chemical and structural stability, only one narrow EPR line, reversible and fast kinetics of oxygen absorption, small time response and a high sensitivity. Oximetry by EPR is based on the modification of the line width with the concentration of oxygen present in the environment of the sample. The χ form of LiPc shows most of the required properties. Nevertheless, it presents different disadvantages⁷: (i) the size of crystals limits the domains of application of oximetry and therefore the oxygen diffusion kinetics; and (ii) the reproducible synthesis of samples having a low concentration of defects is difficult. The polymorphism of LiPc is a crucial problem.

LiPc can be prepared by both chemical and electrochemical routes. The chemical synthesis involves heating of 1,2-dicyanobenzene and lithium metal at 150 °C.¹¹ After completion of the exothermic reaction, the products have been extracted with toluene and LiPc needles have been obtained. The electrochemical method of preparation of LiPc has been first reported by Homborg and Kalz¹² and this has been adopted by several researchers.^{11,13,14} This method involves oxidation of dilithium phthalocyanine (Li_2Pc). A solution has been prepared by dissolving 200 mg of Li_2Pc in 80 ml acetonitrile consisting of 0.1 M tetrabutyl ammonium perchlorate (TBAP).⁶ A two-compartment cell with a porous fritted glass disk separator has been employed. A constant potential of 0.4 V vs. SCE has been applied to a Pt anode and the electrolysis has been continued until the current reduced to a low value. The anode has been reportedly covered with a black powdery deposit, which has got detached from the anode surface and settled at the bottom of the cell container. It is understood from all these studies⁶⁻¹⁴ that the adhesion of

LiPc to the anode substrate is poor and consequently LiPc separates out to form a suspension or powder in the electrolyte. Therefore, preparation of LiPc as a film and its growth as an electrodeposit on the anode has not been possible in these studies. It is anticipated that LiPc deposited electrodes are useful for applications such as electrochromic devices, batteries, fuel cells, sensors etc. Electrodeposited LiPc films on suitable substrates are more desirable for these applications than the electrodes made by coating lipc power using polymeric binders. Additionally, the particle size can also be controlled in the case of electrodeposited film. Furthermore, the preparation technique involves passing of constant current (galvanostatic) through the electrochemical cell in a majority of the above described studies or applying a constant potential (potentiostatic) to the anode in a few studies. Potentiodynamic technique has not been attempted. The quality of the electrodeposits varies with electrochemical technique. For instance, potentiodynamic oxidation of aniline produces polyaniline films of better quality and uniformity than the films prepared by potentiostatic and galvanostatic technique.^{15,16}

The aim of the present work is to electrodeposit LiPc from Li_2Pc as an adherent layer on different anode substrates and to characterize the electrodes. A suitable modification of the supporting electrolyte produces an adherent and thick film of LiPc on Pt and stainless steel (SS) substrates. Potentiodynamic technique is employed in addition to the potentiostatic and galvanostatic techniques for a few studies. Electrochemical and morphological studies of LiPc films are reported.

Experimental

Dilithium phthalocyanine (Aldrich), LiBF_4 (Aldrich), dimethyl sulphoxide (DMSO, Qualigens), acetone (Qualigens) were used for the experiments. Three electrode setup with a Pt foil (0.5 cm^2) or a SS foil (0.72 cm^2) as the working electrode, a large area platinum foil as the counter electrode and a Ag wire as a pseudo reference electrode were used. Potential values are reported against Ag reference electrode. The Ag reference electrode had a stable potential in the electrolyte and the value of potential was 0.19 V against a saturated calomel electrode. Before use the Pt electrodes were treated with conc. HNO_3 , washed with doubly distilled water and rinsed with acetone. The SS electrodes of 5 mm wide and 12 cm length were sectioned out of a commercial grade 304 sheet of 0.2 mm thickness. One end of the electrode was used for deposition of LiPc and the

remaining part was used as the current collector. They were polished with emery, washed and rinsed with acetone. A solution of 30 mM Li_2Pc (15.8 g l^{-1}) in DMSO with 20 mM LiBF_4 (1.9 g l^{-1}) as the supporting electrolyte was prepared. Although a higher concentration of the supporting electrolyte is desirable for electrochemical measurements, low solubility of LiBF_4 in DMSO limited its concentration at 20 mM. Acetone was also used as the solvent in some experiments. A glass cell fitted with ground joints to introduce the electrodes and also to purge the electrolyte with argon gas was used for all experiments. Oxidation of Li_2Pc was carried out by galvanostatic (current density: 2.8 and 6.5 mA cm^{-2}), potentiostatic (potential: 0.8 and 1.0 V) and potentiodynamic (sweep rate: 20 mV s^{-1}) methods. All these methods produced adherent deposits of LiPc on both Pt and SS substrates. After the deposition of LiPc, the electrodes were washed with the solvent and dried at 45°C before using for further experiments. Cyclic voltammetry and ac impedance measurements of LiPc deposited electrodes were carried out in DMSO containing 50 mM LiBF_4 . Electrochemical experiments were carried out using a Ecochemie potentiostat/galvanostat model Autolab 30 and EG&G PARC impedance analyzer model 6310. Electrochemical impedance of LiPc deposited Pt and SS electrodes was measured at their open circuit potentials using 5 mV excitation signal in the frequency range 100 KHz – 10 mHz. Surface morphology of the films was examined by scanning electron microscope (SEM) of model JEOL JSM-840A.

Results and discussions

Cyclic voltammetry of oxidation of Li_2Pc to LiPc.- Figure 1 shows voltammograms recorded by cycling a Pt electrode in Li_2Pc solution in DMSO at several sweep rates. After recording the voltammogram with a particular sweep rate, the Pt electrode was taken out of the cell, cleaned to remove oxidation product on its surface, and reinserted into the cell for recording at another sweep rate. This procedure allowed us to expose the Pt surface for recording voltammograms at each sweep rate. During the forward direction of the sweep, anodic current peaks appear at about 0.44 - 0.52 V before reversing the sweep direction at 0.8 V. In the reverse direction of the potential sweep, there are broad, minor cathodic peaks at about 0.3 V. The cathodic peak is smaller than the anode peak by several times, and the ratio of these two peak currents remains nearly the same at all sweep rates. A large ratio of the peak currents with a wide potential

separation of the anodic and the cathodic peaks is considered to correspond to an irreversible or quasi reversible oxidation. Accordingly the anodic peak is ascribed due to oxidation of Li_2Pc .

Cyclic voltammetry of Li_2Pc has been rarely reported in the literature.¹³ Voltammograms of Li_2Pc dissolved in acetonitrile consisting of TBAP as the supporting electrolyte over a wide positive potential range comprise basically two processes. The first process occurring at low potentials is quasi reversible and the second process at higher potentials is an irreversible oxidation. The region of voltammograms corresponding to the quasi reversible oxidation¹³ is similar to the data shown in Fig.1. The second irreversible oxidation was also observed in the present study when the voltammograms were recorded encompassing higher potentials (not shown) thus confirming that the data obtained in the present work is comparable to the study of Ilangovan et al.¹³ However, these authors¹³ have reported sharp anodic and cathodic peaks of equal magnitude when cyclic voltammograms were recorded at 10 mV s^{-1} sweep rate. The ratio of the anodic peak current to the cathodic peak current remains nearly unity with an increase of sweep rate. This result is in contradictory to the data shown in Fig. 2, where the ratio of the peak currents does not approach to unity even at low sweep rates. According to the study of Ilangovan et al.,¹³ the cyclic votammogram recorded at 10 mV s^{-1} shows a steep increase of current at the start of the anodic peak with full width at half-maximum narrow, about 38 mV. This value is comparable neither with 90.6 mV reported for a surface wave without any interaction among the adsorbate nor with 28 mV corresponding to a solution-phase redox process. During the cathodic sweep, an overlap between the forward and reverse sweeps leading to a current loop has been noticed. The presence of current loop is known to correspond to the nucleation and growth mechanism of electrodeposition processes.¹⁷ Unlike these features, current peaks of the present study (Fig. 1) do not overlap and the full width at half-maximum obtained at 10 mV s^{-1} is 132 mV. The difference in various features of voltammograms of Ilangovan et al.,¹³ and the present study (Fig. 1) is attributed to different supporting electrolytes used. With an increase in sweep rate (Fig. 1), there is an increase in the anodic peak current and also there is a positive shift in the anodic peak potential (E_{pa}), which is a characteristic feature of an irreversible reaction. A plot of peak current versus $v^{1/2}$, where v is the sweep rate, is

seen to be linear (Fig. 2(a)), which suggests that the oxidation of Li₂Pc to LiPc is diffusion controlled. The relationship between E_p and v for an irreversible reaction is given by Eq. (1)

$$E_p = K + (2.303RT / 2\alpha_a n_a F) \log v \quad (1)$$

where K is a constant; α_a , the transfer coefficient; n_a , the number of electrons transferred up to the rate determining step of the oxidation; and the other symbols have their usual meanings. The product $(2.303RT / \alpha_a n_a F)$ is equivalent to the Tafel slope. The value of α_a of the oxidation of Li₂Pc can be evaluated using Eq. (1). A plot of E_p versus $\log v$ is shown in Fig. 2(b). The value of $(dE_p/d\log v)$ obtained is 0.082. Accordingly the Tafel slope has a value of 0.164 V and thus the value of $(\alpha_a n_a)$ is 0.36. Since the value of n_a is unity, the value of α_a is 0.36. This value is less than 0.5 reported.¹³

Cyclic voltammetric oxidation of Li₂Pc was also studied on SS. Voltammograms recorded at a few sweep rates, and also the voltammograms recorded on Pt and SS at 20 mV s⁻¹ sweep rate for comparison are shown in Fig. 3. At slow sweep rates, there is a broad current peak at about 0.6 V on SS (Fig. 3(a)) during the forward sweep, but peaks do not appear at sweep rates > 20 mV s⁻¹. The cathodic peak appearing during the reverse sweep is negligibly smaller in comparison with the anodic peak. This feature is common for both Pt and SS anodes. A comparison of the voltammogram of Pt and SS (Fig. 3(b)) suggests that the oxidation current is lower and the reaction occurs at a higher (> 0.2 V) overpotentials on the SS anode in relation to Pt. However, the cathodic peak appears at about 0.30-0.35 V for both electrodes. The difference in voltammograms of Pt and SS electrodes could be due to the fact that the surface of SS substrate is covered with an oxide passive film. Nevertheless, it was found that adherent deposits of LiPc are formed on SS surface also, as discussed below.

Deposition of adherent films of LiPc on Pt and SS.- Galvanostatic, potentiodynamic and potentiostatic methods were employed for the deposition of LiPc films. It was found that all these methods produced adherent films of LiPc on both Pt and SS electrodes. The potentiodynamic method involved cycling of the electrodes at a known sweep rate repeatedly between 0 and 0.8 V. As discussed in the previous section, the quasi-reversible oxidation peak appearing at Pt electrode corresponds to the formation of LiPc. This oxidation product is not soluble in the organic medium and therefore

deposits on the anode. Due to the extended nature of LiPc, a significant stabilization of the solid takes place through intermolecular interactions. A thin layer of LiPc forms on the electrode during the initial cycles, and thereafter the layer grows in thickness. The LiPc deposit does not separate out of the substrate. The thickness depends on the number of cycles. For instance at a sweep rate of 20 mV s^{-1} , a thickness of about $14 \text{ }\mu\text{m}$ was obtained after repeated 40 cycles. It was found that the cyclic voltammograms recorded during deposition of LiPc were similar to those shown in Fig. 1 at a given sweep rate. Also, the LiPc deposits were adherent to the substrate when deposited potentiostatically at 0.8 and 1.0 V; and galvanostatic condition at 2.8 and 6.5 mA cm^{-2} . Although the oxidation of Li_2Pc on SS occurs at slower rates and higher potentials than on Pt (Fig. 3), it was found that the LiPc deposits on SS by the three electrochemical methods were also quite adherent and stable.

In contrast to the present results, the formation of LiPc with poor adherence on the anode has been reported in several publications.⁶⁻¹⁴ In all these studies, TBAP has been employed as the supporting electrolyte in either acetone or acetonitrile. In the present study also, a few potentiodynamic experiments were carried out using TBAP in DMSO consisting of Li_2Pc . It was found that LiPc deposits on both Pt and SS anodes were poorly adhered and the crystals settled at the cell bottom, thus confirming the results reported in the literature.⁶⁻¹⁴ However, stable and adherent films of LiPc on the anode were obtained subsequent to changing of the supporting electrolyte from TBAP to LiBF_4 . Furthermore, it was found that when the solution consisting of Li_2Pc and TBAP in DMSO or acetone was left undisturbed overnight, formation of crystals of LiPc by chemical oxidation was observed. However formation of LiPc did not take place if a solution of Li_2Pc in DMSO or acetone consisting of LiBF_4 was left undisturbed for several days. Although air oxidation of Li_2Pc powder is known to occur, it is unlikely that it occurs in solution state as evident from the solution consisting of LiBF_4 . It is therefore inferred that TBAP acts as an oxidizing agent for the oxidation of Li_2Pc to LiPc. Due to the combined effect of oxidizing action of TBAP and anodic potentials, the adherence of electrodeposited LiPc to the substrate is poor. By replacing TBAP with LiBF_4 as the supporting electrolyte in the present study, the adhesion between LiPc and the anode improves and therefore stable films of LiPc are obtained. Additionally, the difference in

the nature of cyclic voltammograms of the present study (Fig. 1) from those reported using TBAP as the supporting electrolyte¹³ with different values of transfer coefficient suggests a different nucleation and growth mechanism, which favors the adherence of LiPc crystals to the substrate.

Cyclic voltammetry of LiPc Films on Pt and SS.- Although electrochemically synthesized LiPc has been subjected to optical and magnetic studies extensively, there has been no report on electrochemical studies. Electrochemical studies of LiPc are considered important in view of its applications in electrochromic devices, batteries, etc. The only electrochemical characterization study to the best of authors' knowledge is reported by Turek et al.⁶ In this study, the electrochemically prepared LiPc has been dissolved in a mixture of tetrahydrofuran and chloronaphthalene as a solvent with TBAP as the supporting electrolyte. Cyclic voltammogram of a Pt electrode in this electrolyte has been shown to comprise two reversible redox peaks. The pair of current peaks at about 0.17 V vs. SCE has been attributed to reversible $\text{LiPc}^{\cdot-} / \text{LiPc}^{\cdot-}$ process, and the other pair of current peaks to reversible $\text{LiPc}^{\cdot-} / \text{LiPc}^{\cdot-}$ process. Cyclic voltammetry or any other electrochemical characterization studies of LiPc films have not been reported in the literature.

The Pt and SS electrodes deposited with 14 μm thick LiPc films by potentiodynamic method were subjected to cyclic voltammetry in a 50 mM LiBF_4 solution of DMSO between 0 and 0.5 V. Voltammograms of the LiPc/Pt and LiPc/SS electrodes are shown in Fig. 5. A pair of current peaks is observed for LiPc/Pt electrode in the potential region between 0.25 and 0.30 V (Fig. 5(a)). A comparison of the voltammograms obtained during deposition of LiPc (Fig. 1) with Fig. 5(a) reveals that the magnitude of current in Fig. 5(a) is lower and the peaks appear at less anodic potentials than in Fig. 1. The ratio of the anodic peak current to the cathodic peak current is close to unity in Fig. 5(a) unlike the larger anodic peak current than the cathodic peak current in Fig. 1. The anodic and cathodic peaks in Fig. 5(a) are separated by about 60 mV, and the peak potentials are invariant with sweep rate. These are characteristic features of a reversible electrochemical reaction.¹⁸ A plot of peak currents versus $v^{1/2}$ is found to be linear as shown in Fig. 5(b). These observations suggest that the electrochemical reaction corresponding to the pair of current peaks (Fig. 5(a)) is diffusion controlled, which

involves an electrolyte species. If the reaction corresponds to only the electron-transfer process in LiPc film on Pt such as $\text{LiPc}^\cdot / \text{LiPc}^-$, the peak potential separation of the anodic and cathodic peaks is expected to be close to zero, and such a voltammogram is known as a surface wave.¹⁸ The reversible $\text{LiPc}^\cdot / \text{LiPc}^-$ process was proposed when LiPc was dissolved in a suitable solvent.⁶ Since in the present study LiPc is present as a film on the electrode, and the peak potential separation is close to 60 mV (Fig. 5(a)), it is likely that the corresponding reaction is $\text{LiPc} / \text{Li}_2\text{Pc}$, which involves Li^+ ions present in the electrolyte. It is therefore likely that the $\text{LiPc}/\text{Li}_2\text{PC}$ reversible process occurs in the potential region between 0.25 and 0.30 V.

Cyclic voltammograms of LiPc/SS electrode recorded in 0.2-0.8 V range at several sweep rates are shown in Fig. 5(c). It is interesting to note that LiPc deposited on SS does not exhibit current peaks in contrast to the well defined peaks of LiPc/Pt electrode (Fig. 5(a)). Thus it is inferred that although an adherent deposit of LiPc is formed on the SS substrate, it does not possess electrochemical activity. Furthermore, the voltammograms recorded at several sweep rates are rectangular in shape and current increases with increase of sweep rate, which are characteristic features of a capacitor material.¹⁹ A plot of current versus v (Fig 5(d)) is linear confirming capacitor property of LiPc/SS electrode. From the slope of the linear plot, the value of capacitance obtained is $64 \mu\text{F cm}^{-2}$.

It is interesting to note that adherent films of LiPc can be deposited in the present study on both Pt and SS substrates, and the crystallographic (Fig. 4) as well as morphological (as discussed below) properties of LiPc on both substrates are nearly similar. However, the electrochemical activity of LiPc/Pt is different from LiPc/SS. The presence of oxide film on the surface of SS underneath LiPc, and also the higher potentials required for the oxidation of Li_2Pc to LiPC on SS could be the reasons for different electrochemical properties.

Ac impedance of LiPc/Pt and LiPc/SS electrodes.- Electrochemical impedance measurements provide a range of useful information of electrode electrolyte interface.²⁰ In the present study, LiPc/Pt and LiPc/SS electrodes were subjected to impedance measurements in LiBF_4 solution. Nyquist plots of impedance spectra are shown in Fig. 6. The spectrum of LiPc/Pt electrode is characterized by a semicircle, which is a

characteristic feature of a parallel combination of interfacial resistance and double-layer capacitance (Fig. 6, curve 1). Electrochemical impedance studies of platinum phthalocyanine (PtPc) in acetonitrile electrolytes have been recently reported.²¹ The impedance spectrum consists of high frequency intercept on the real axis, a semicircle in the high frequency range, a Warburg region in the mid frequency range and a capacitive behavior at low frequencies. However, in the case of LiPc of the present study (Fig. 6, curve 1), only a distorted semicircle is observed without Warburg and capacitive regions. The high frequency intercept of the semicircle provides the ohmic resistance and a value of 264 Ω is obtained from both curves in Fig. 6. The ohmic resistance includes the resistances of the electrolyte, electrode substrate, electrodeposited LiPc film, electrical leads, etc. The diameter of the semicircle provides the value of charge-transfer resistance (R_{ct}). The double-layer capacitance (C_{dl}) can be calculated from the frequency (f^*) corresponding to the maximum of the semicircle using the equation, $C_{dl} = 1/(2 \pi f^* R_{ct})$. Approximate values of interfacial resistance and double layer capacitance obtained from the data of LiPc/Pt electrode (Fig. 6, curve 1) is 33.2 $k\Omega \text{ cm}^2$ and 96 $\mu\text{F cm}^{-2}$, respectively. These values are only approximate as the semicircle (Fig. 6, curve 1) is distorted and a rigorous analysis is required to obtain the accurate values. The impedance spectrum of LiPc/SS (Fig. 6, curve 2) does not take the shape of a semicircle. It appears that the data constitute a segment (arc) of a large semicircle. By fitting the arc to a semicircle, a value of 0.9 $M\Omega \text{ cm}^2$ is obtained for interfacial resistance of LiPc/SS electrode. Thus the interfacial resistance of LiPc/SS is several times higher than the LiPc/Pt electrode. These features of impedance spectra agree well with the inferences obtained from the cyclic voltammetric experiments (Fig. 5).

The effect of treatment in dil. H_2SO_4 . - In the view of several applications of LiPc coated electrodes, it was intended to study the stability of these films in an aqueous solution. The electrochemical stability of LiPc films were investigated by treating a LiPc/Pt electrode in a dilute acidic medium. The electrode was dipped in 0.05 M H_2SO_4 for 3 h, washed, dried and soaked in a $LiBF_4$ solution in DMSO for 1 h before recording cyclic voltammograms and electrochemical impedance spectra (Fig. 7). The redox activity of LiPc is lost after treatment in dil. H_2SO_4 as evidenced from the absence of current peaks (Fig. 7(a)). This feature is also evident from an increase in interfacial

resistance in the impedance spectrum (Fig. 7(b)). It is likely that Li^+ present in LiPc is exchanged with H^+ in the acidic electrolyte resulting in the formation of HPc due to the treatment in dil. acidic solution. Another possible reason is change in crystalline structure of LiPc film. The micrographs of LiPc/SS treated in dil H_2SO_4 appeared as amorphous.

Microstructure of LiPc films.- Microstructural characterization of LiPc has been of recent interest in the literature.^{13,14,22} Thin films of LiPc have been grown on a glass substrate and exposed to acetone vapors.¹⁴ The morphology of LiPc films has been shown to change drastically from amorphous to needle-like crystallites on exposing to acetone vapors. Powders of LiPc obtained by electrochemical oxidation of Li_2Pc have been examined for microstructure.¹³ The powders showed needle-shaped crystals suggesting one dimensional growth of LiPc. Thin films of LiPc have been electrochemically grown on indium tin oxide (ITO) glass substrate and the morphology was examined.²¹ In the initial stages of deposition (< 2 min), the LiPc films consist of a random distribution of needles lying in the plane of the substrate. For >10 min deposition, an unidirectionally oriented very long microcrystallites (up to several hundred μm) are formed. The unidirectional ordering of crystallites has been attributed to the existence of a hydrodynamical flow of solvent on the surface of the film during deposition.

Microstructure of LiPc coated SS and Pt electrodes were examined at different stages of deposition by potentiodynamic and potentiostatic method. The micrographs of LiPc/SS electrodes prepared potentiodynamically at 20 mV s^{-1} sweep rate for different number of cycles are shown in Fig. 8. After deposition of LiPc by 5 potential sweeps (Fig. 8(a)) at 20 mV s^{-1} , short needle-like crystals are formed on the SS surface in a random way. The average length of the needles is about $10 \mu\text{m}$ with thickness less than $1 \mu\text{m}$. The deposit has a low coverage on the substrate, as the surface of bare SS is largely seen. On increasing the number of sweeps to 40 (Fig. 8(b)) at 20 mV s^{-1} , the deposition coverage increases and no bare SS surface is noticed. The needles of LiPc grow in length and also thickness resulting in lengthy fibers. There is random two dimensional growth, which leads to the formation a non-woven like structure by joining of neighboring needles (Fig 8(b)). The microstructure of the electrode prepared from 40 cycles at 100 mV s^{-1} is similar to the electrode prepared at 20 mV s^{-1} (Fig. 8(b)). However, the fibers

are thinner and the deposit has finer porosity (Fig. 8(c)) in comparison with the microstructure of the deposit prepared at 20 mV s^{-1} (Fig. 8(b)).

The microstructure of LiPc/SS prepared potentiostatically at 0.9 and 1.2 V are compared in Fig. 9. The deposit prepared at 0.9 V (Fig. 9(a)) has large voids with nearly straight rod shaped crystals. On the other hand, the material deposited at 1.2 V has thinner and larger fibers oriented two dimensionally and it has finer porosity (Fig. 9(b)). Oxidation of Li_2Pc to form LiPc deposit occurs at a faster rate at 1.2 V than at 0.9 V. It is inferred that faster rate favors dense deposits of LiPc with long and thin fibers covering the surface uniformly.

The microstructure of LiPc/Pt electrodes are shown in Fig. 10. After 5 potential cycles the micrograph of LiPc/Pt (Fig. 10(a)) shows needle-like crystals with higher coverage on the Pt surface than on SS (Fig. 8(a)). This is probably due to higher rate of deposition of LiPc at lower potentials on Pt than on SS as reflected in the cyclic voltammograms (Fig. 3(b)). By increasing the number of potential sweeps, the needles grow longer and thicker with increased coverage (Fig. 10(b)). The microstructures of LiPc on Pt substrate (Fig. 10) is nearly similar to those obtained on SS substrate, thus, suggesting a negligible influence of the substrate on microstructure although the substrate effects are present on the rate of LiPc deposition as well as its electrochemical activity.

SEM micrographs of LiPc/SS prepared potentiodynamically in acetone medium were also recorded. The exterior surface of a thick deposit of LiPc prepared from acetone resembled to the micrograph of LiPc prepared from DMSO (Fig. 8). The interior layer recorded in an expanded view showed rod-like crystals grown perpendicular to the substrate, and the exterior layer consisted of rods grown parallel to the surface over the interior layer.

Conclusions

Electrooxidation of Li_2Pc in DMSO or acetone consisting of LiBF_4 as the supporting electrolyte produces LiPc on Pt or SS substrates. Unlike the formation of non-adherent, powdery deposits of LiPc reported in the literature using TBAP as the supporting electrolyte, the present experimental conditions using galvanostatic, potentiostatic and potentiodynamic techniques favor the formation of adherent deposits. The reason for obtaining adherent films is attributed to using LiBF_4 as the supporting electrolyte instead

of TBAP. The kinetics of electrodeposition varies with the substrate (Pt or SS) used for the deposition. Also, the electrochemical properties of LiPc/Pt and LiPc/SS electrodes are different. Nevertheless, there are similarities in the microstructure of LiPc deposited on both Pt and SS. The adherent films of LiPc on metallic substrate are expected to be useful in several applications. The capacitive behaviour of LiPc/SS electrodes suggests a potential use of them in electrochemical supercapacitors. Several investigations of adherent LiPc films are underway in our laboratories.

References

1. T.J.Marks, *Science*, **227**, 881 (1985).
2. T. Inabe and H. Tajima, *Chem. Rev.*, **104**, 5503 (2004).
3. C.J. Schramm, R.P. Scaringe, D.R. Stojakovic, B.M. Hoffman, J.A. Ibers and T.J. Marks, *J. Am. Chem. Soc.*, **102**, 6702 (1980).
4. P. Turek, P. Petit, J.-J. Andre, J. Simon, R. Even, B. Boudjema, G. Guillaud and M. Maitrot, *J. Am. Chem. Soc.*, **109**, 5119 (1987).
5. R.D. Gould, *Coord. Chem. Rev.*, **156**, 237 (1996).
6. P. Turek, J.-J. Andre, A. Giraudeau and J. Simon, *Chem. Phys. Lett.*, **134**, 471 (1987).
7. J.J. Andre and M. Brinkmann, *Synth. Met.*, **90**, 211 (1997).
8. G. Ilangovan, J.L. Zweier and P. Kuppusamy, *J. Phys. Chem. B*, **104**, 9404 (2000).
9. M. Brinkmann, C. Chaumont, H. Wachtel and J.-J. Andre, *Thin Solid Films*, **283**, 97 (1996).

10. G. Ilangovan, R. Pal, J.L. Zweier and P. Kuppusamy, *J. Phys. Chem. B.*, **106**, 11929 (2002).
11. M. Dumm, M. Dressel, M. Nicklas, P. Lukenheimer, A. Loidl, M. Weiden, F. Steglich, B. Assmann, H. Homborg, and P. Fulde, *Euro. Phys. J. B.*, **6**, 317 (1998).
12. H. Homborg and W. Kalz, *Naturforsch.*, **33b**, 1067 (1978).
13. G. Ilangovan, J.L. Zweier and P. Kuppusamy, *J. Phys. Chem. B.*, **104**, 4047 (2000).
14. M. Brinkmann, J.C. Wittmann, C. Chaumont, J.J. Andre, *Thin Solid Films.*, **292**, 192 (1997).
15. K.R. Prasad and N. Munichandraiah, *J. Electrochem. Soc.*, **149**, A1393 (2002).
16. S. M. Park in H.S. Nalwa (Ed.), *Handbook of Organic Conductive Molecules and Polymers*, Vol. 2, p. 504, Wiley, New York (1997).
17. R. Greef, R. Peat, L. M. Peter, D. Pletcher and J. Robinson, *Instrumental Methods in Electrochemistry*, Ellis Horwood (1995).
18. A.J. Bard and L.R. Faulkner, *Electrochemical Methods*, John Wiley (1980).
19. B. E. Conway, *Electrochemical Supercapacitors*, Kluwer Academic/Plenum Publishers, New York (1999).
20. J. R. Macdonald, *Impedance Spectroscopy*, John Wiley & Sons, New York (1987).
21. J. Jiang and A. Kucernak, *J. Electroanal. Chem.*, **514**, 1 (2001).
22. J.J. Andre and M. Brinkmann, *Synth. Met.*, **121**, 1359 (2001).

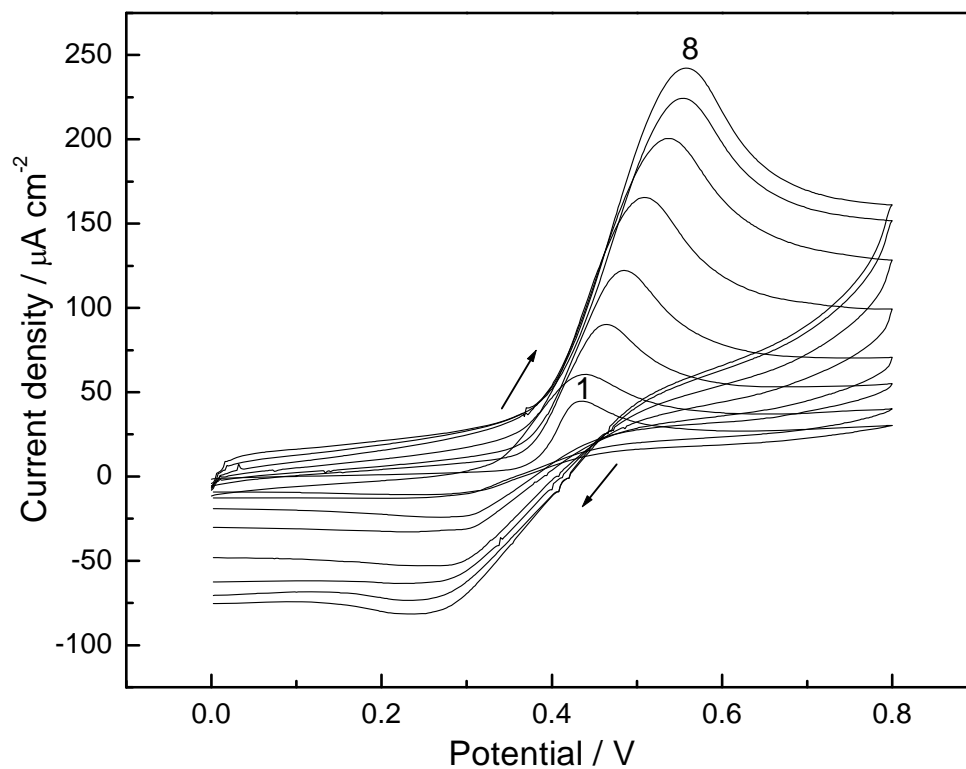


Fig. 1. Cyclic votammograms of a Pt electrode in 30 mM Li_2PC in DMSO consisting of 20 mM LiBF_4 at a sweep rate of (1) 2, (2) 5, (3) 10, (4) 20, (5) 40, (6) 60, (7) 80 and (8) 100 mV s^{-1} .

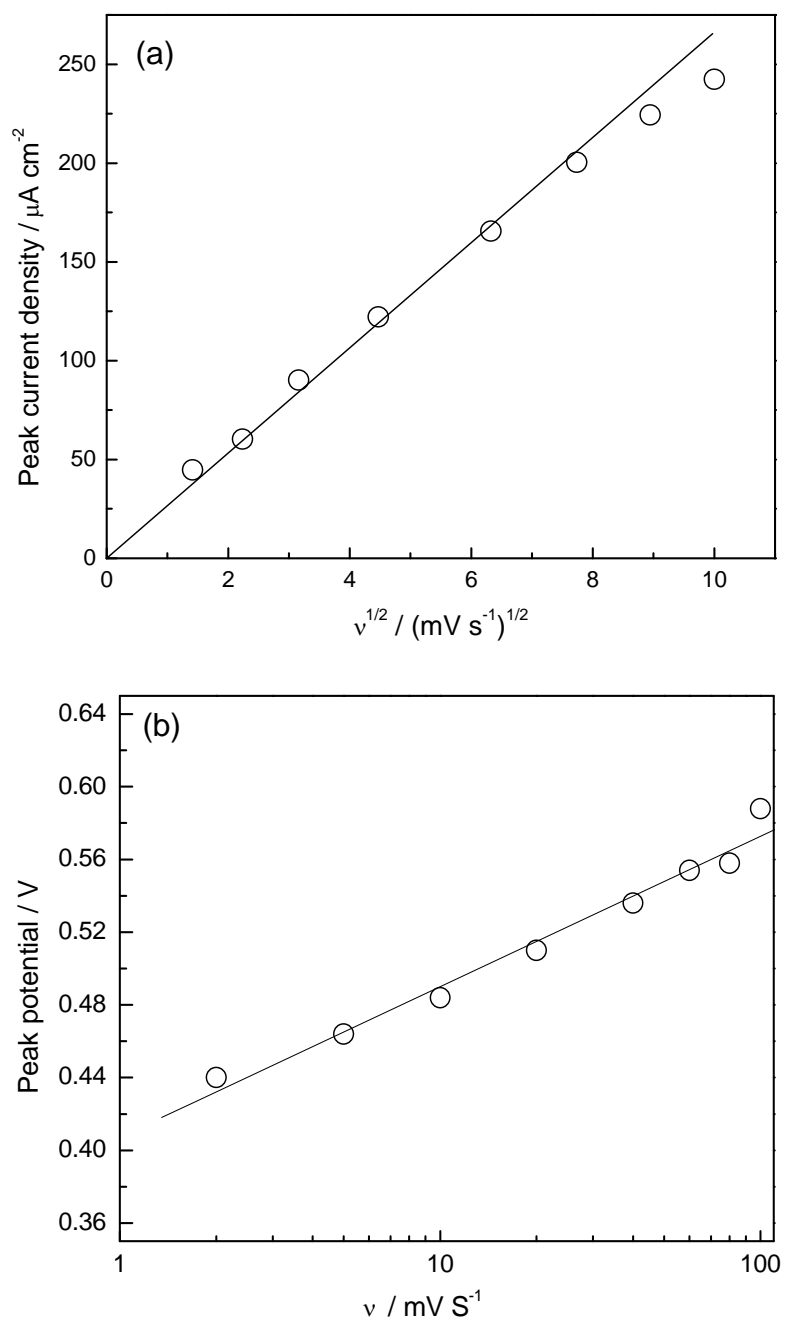


Figure 2. Variations of (a) peak current density with square root of sweep rate ($v^{1/2}$) and (b) peak potential with sweep rate (v) for the cyclic voltammograms shown in Fig. 1.

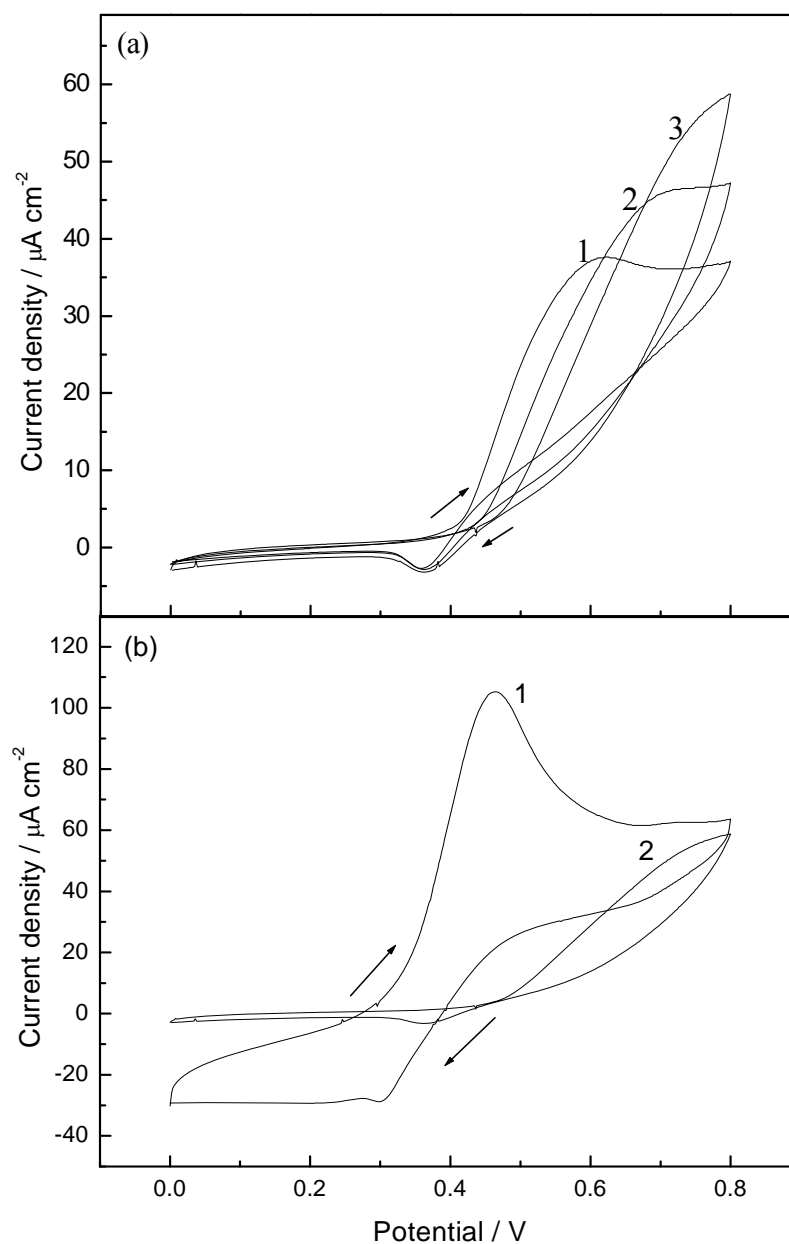


Figure 3. (a) Cyclic voltammograms of a SS electrode in 30 mM Li_2Pc in DMSO consisting of 2 mM LiBF_4 at a sweep rate of (1) 5, (2) 10 and (3) 20 mV s^{-1} , and (b) Pt (1) and SS (SS) electrodes at 20 mV s^{-1} for comparison

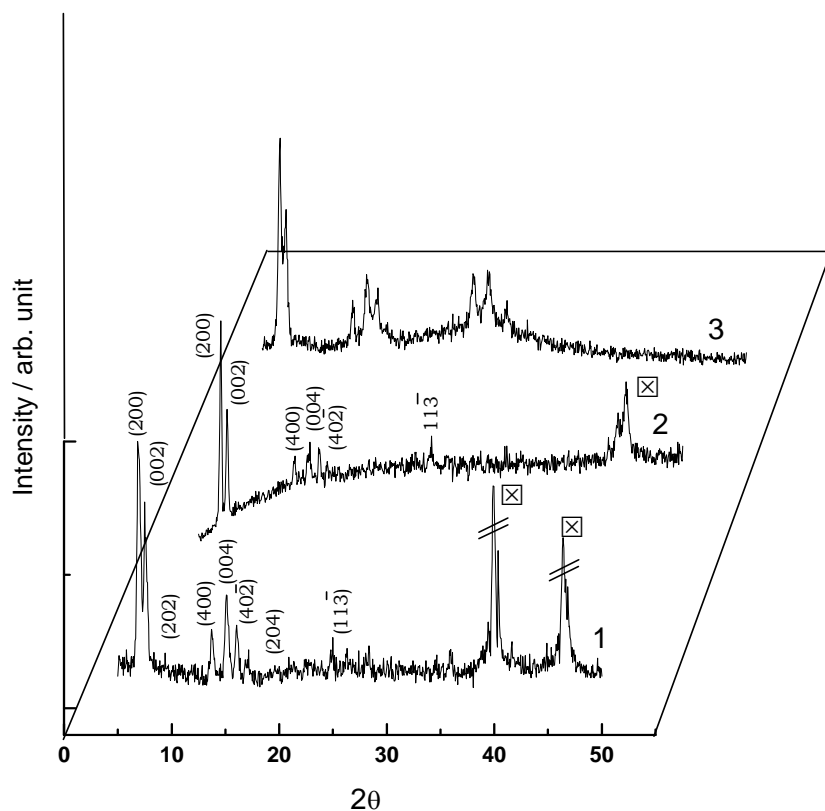


Figure 4. Powder XRD patterns (source: $\text{Cu K}\alpha$) of (1) LiPc/Pt, (2) LiPc/SS and (3) LiPc powder obtained from chemical oxidation of Li_2Pc by TBAP. Patterns 1 and 2 are indexed to monoclinic α -phase, and pattern 3 corresponds to a mixed phase. The peaks marked [x] correspond to the reflections of the substrates – Pt (pattern 1) and SS (pattern 2).

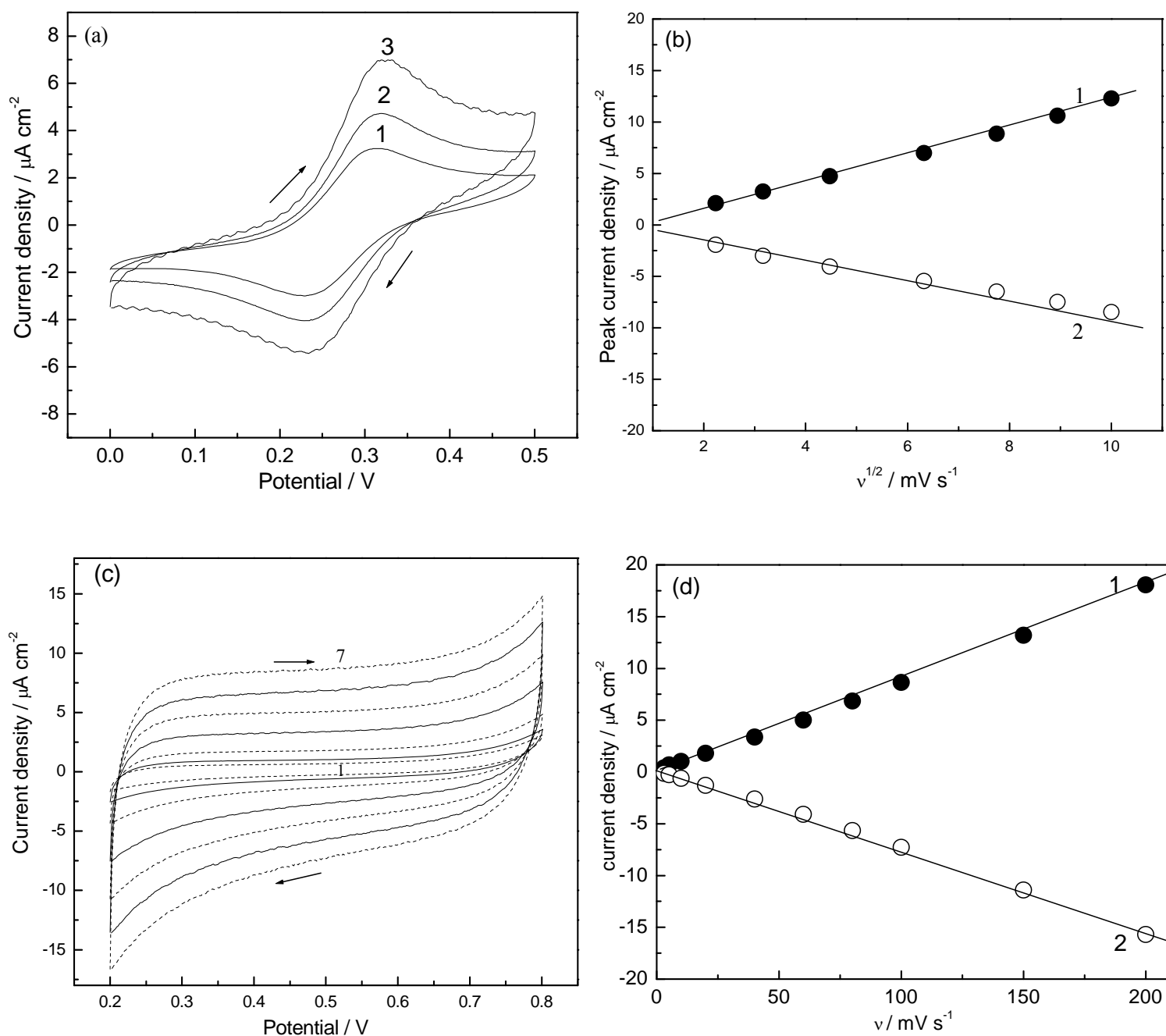


Figure 5. (a) Cyclic voltammograms of a LiPc/Pt electrode in DMSO consisting of 50 mM LiBF₄ at a sweep rate of (1) 5, (2) 10 and (3) 20 mV s⁻¹; (b) variation of (1) anodic and (2) cathodic peak current density with square root of sweep rate ($v^{1/2}$) of the data in (a); (c) cyclic voltammograms of a LiPc/SS electrode in DMSO consisting of 50 mM LiBF₄ at a sweep rate of (1) 5, (2) 10, (3) 20, (4) 40, (5) 60, (6) 80, (7) 100 mV s⁻¹; and (d) variation of (1) anodic and (2) cathodic current density at 0.5 V obtained from (c) with sweep rate (v).

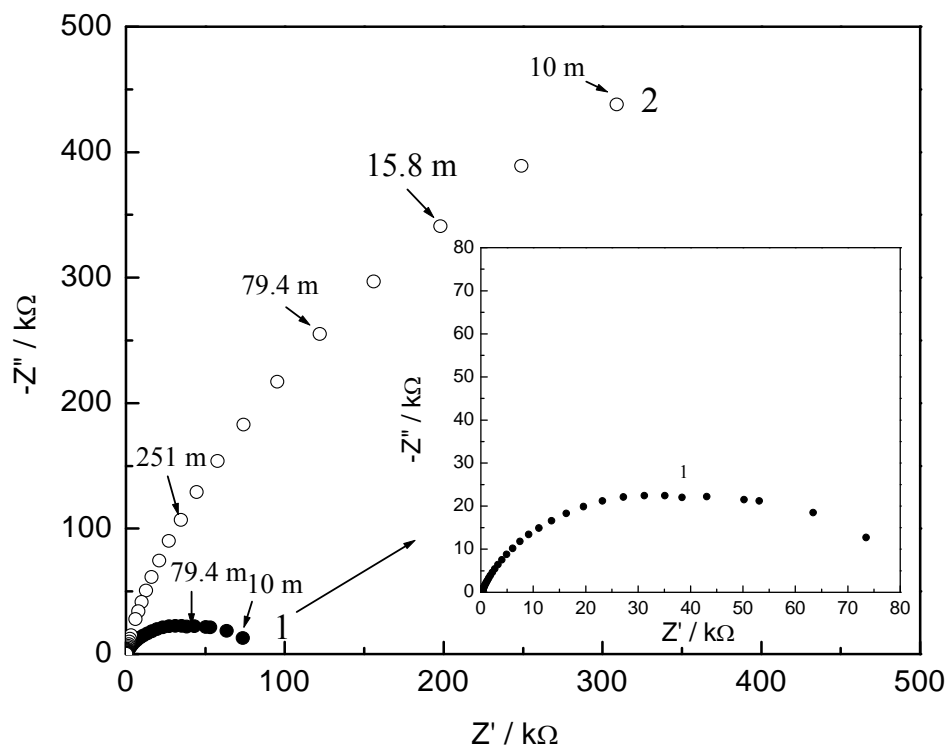


Figure 6. Nyquist impedance plot of (1) LiPc/Pt and (2) LiPc/SS electrodes in 50 mM LiBF₄. Curve 1 is expanded and shown as inset. Frequency values of some data points are given in Hz.

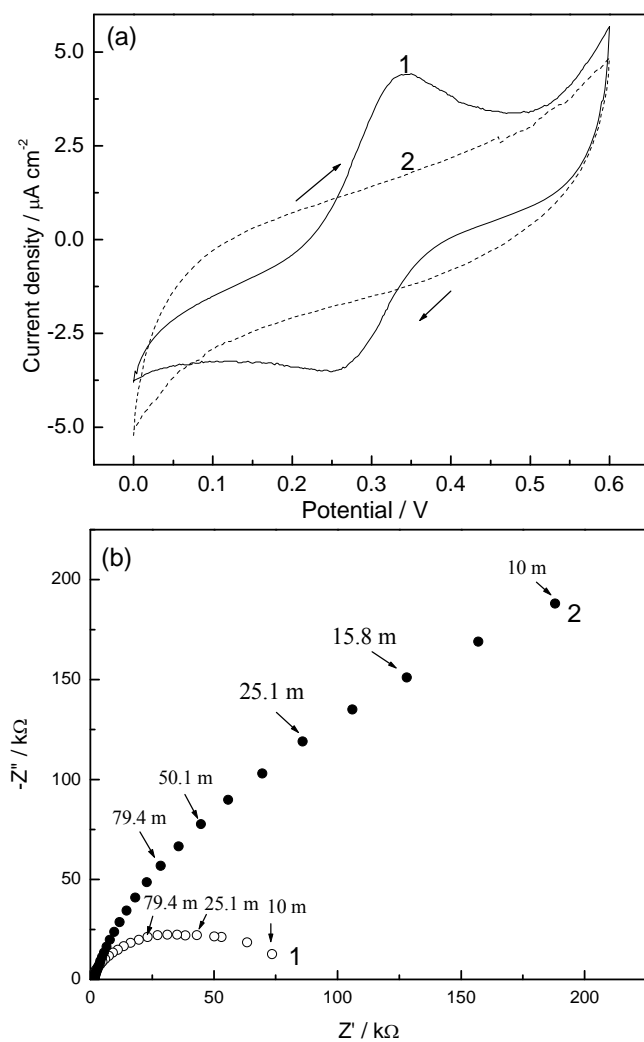


Figure 7. (a) Cyclic voltammograms and (b) electrochemical impedance Nyquist plots of a LiPc/Pt electrode in 50 m M LiBF_4 (1) before and (2) after treatment in 50 M H_2SO_4 .

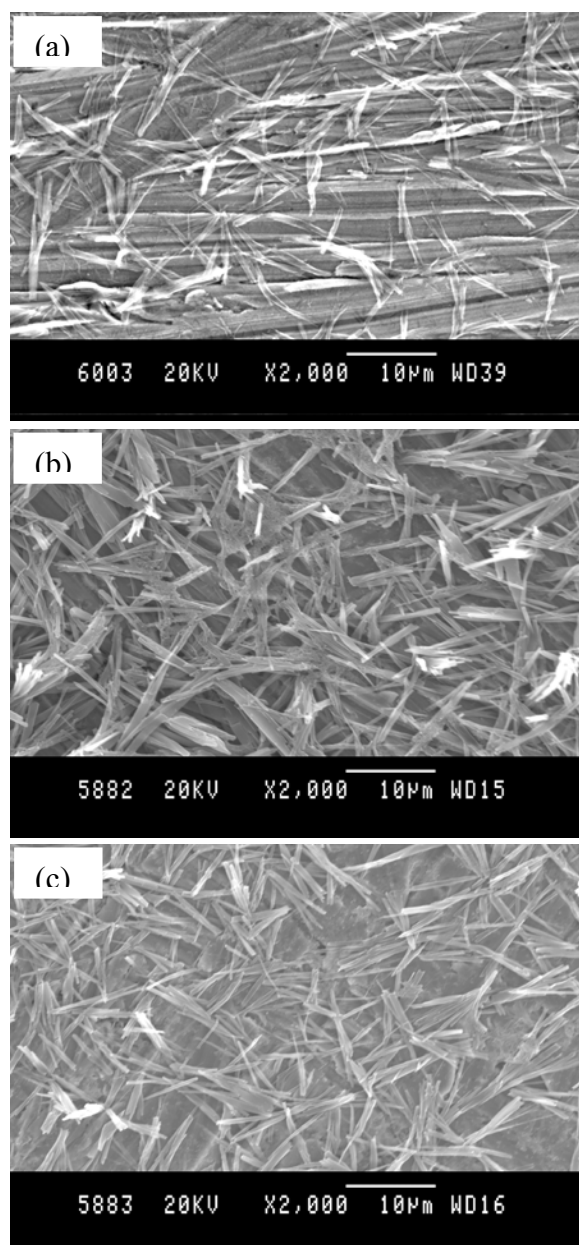


Figure 8. Scanning electron micrographs of LiPc deposited on SS electrodes after (a) 5 sweeps at 20 mV s^{-1} , (b) 40 sweeps at 20 mV s^{-1} and (c) 40 sweeps at 100 mV s^{-1} preparation in 20 mM Li_2Pc in DMSO consisting of 20 M LiBF_4 .

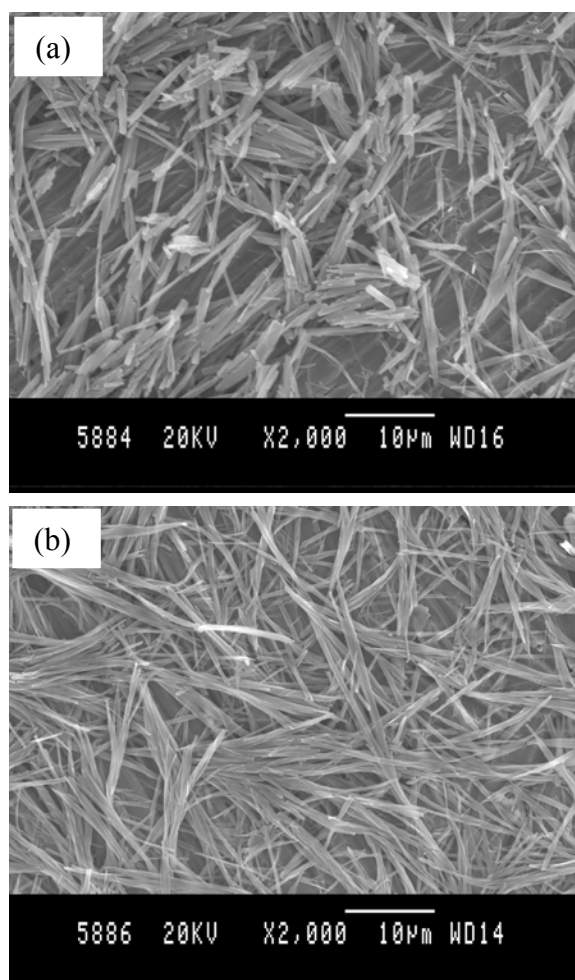


Figure 9. Scanning electron micrographs of LiPc deposited on SS potentiostatically at (a) 0.8 V for 1 h and 1.0 V for 1 h.

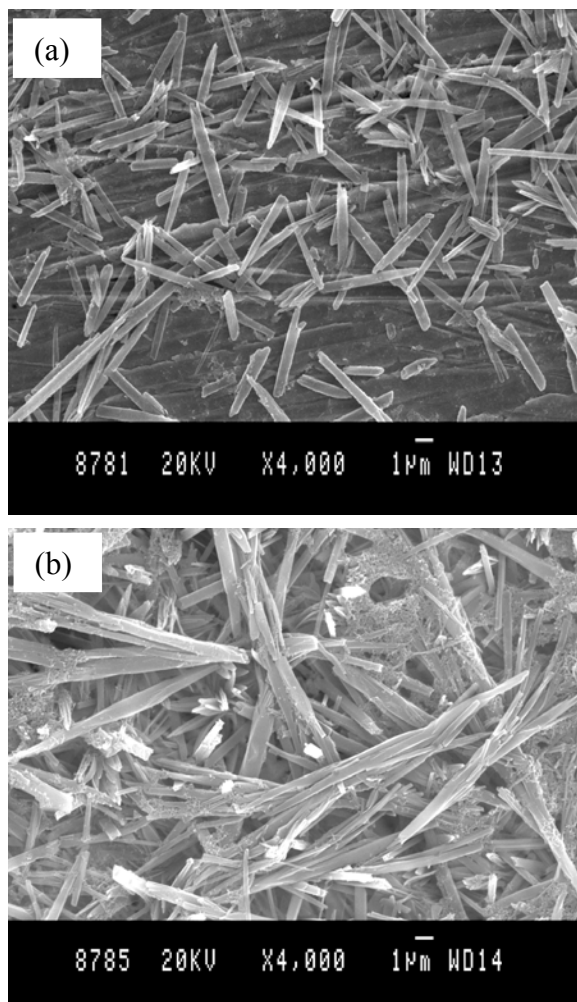


Figure 10. Scanning electron micrographs of LiPc deposited on Pt potentiodynamically at 20 mV s^{-1} for (a) 5 sweeps and (b) 40 sweeps.

3. Studies on composite of dilithium phthalocyanine and iodine

Dopant induced conductivity modulation is of great interest in semiconductor technology. Modifications of organic materials with several dopants have extended applications. Strong oxidizing agents like iodine, bromine, chlorine were doped in metal phthalocyanines to improve p type conductivity. Removal of an electron from the HOMO creates a hole. There are various approaches adapted for doping such as co-evaporation, vapour phase doping, solid-state doping, etc. Phthalocyanine systems are very well studied for its p type doping. Controlled doping followed by variation in conductivity is studied. Dopants form charge transfer salts, which are deeply colored, and they are highly sensitive to air and light. Charge delocalization in organic semiconductors and in macrocyclic molecules affects their conductivity. Linear stacking of dopant, planarity and their π electron delocalization along with molecule greatly enhance the conductivity. Doped TCNQ exhibits metallic type conductivity. Long range order and mobility of charge carriers in the planar molecule are affected by the dopants like I_2 . Iodine doped phthalocyanines are found to have I_3^- stacked along parallel channels of phthalocyanine. This reduces effective π electron overlap of these ring system. Tetra cyano-substituted phthalocyanine is also used as an efficient cathode material. These phthalocyanine molecules shows polymorphism and depending upon the crystal structure the charge transport in these system varies. In the present study, the effect of iodine doped in Li_2Pc was studied by impedance, and other spectral and XRD studies. The effect of temperature on the I_2 doped Li_2Pc was also studied.

Experimental

I_2 doped Li_2Pc was prepared by solid-state mixing of Li_2Pc (recrystallized) and I_2 (Fluka) in different molar ratio. The sample was mixed for 12 hours before making a pellet. Cells were assembled with the pellets sandwiching between two symmetrical stainless steel (SS) electrodes, in Argon filled glove box (MBraun-Unilab). The time dependent and also temperature dependent impedance measurement were recorded. Different concentrations of I_2 were doped in Li_2Pc and the maximum concentration of I_2 was limited to 20%. Impedance spectra were measured with EG&G (model 6310) and Solartron (model 1287) in the frequency range of 100 KHz to 10 mHz. Infrared and UV-

Vis spectra were recorded for the I_2 doped samples by mixing the sample with dry KBr. XRD measurements were also performed.

Result and Discussion

Temperature effect showed an increase in impedance, both for the high frequency and low frequency semicircles (Fig. 1). In oxygen doped thin film of other metal phthalocyanine, there was an increase in the impedance observed with temperature. This was attributed to the desorption of the oxygen from the film. Figure 2 shows nearly reversible room temperature conductivity before and after heating experiment shows there is no desorption of I_2 molecule from the pellet on heating. But a decrease in the impedance is observed as shown in the Fig. 2(b). Charge delocalization in the organic solids is influenced by the long range order and effective intermolecular stacking. Using planar molecule which can stack in the direction along the molecular system improve the charge delocalization. The effective overlap is affected by the size, planarity, stacking directions of dopant molecule.

Temperature dependent impedance measurements of the undoped Li_2Pc shows decrease in the impedance values for both 1st and 2nd semicircle with temperature (Fig. 3). In contrast, all I_2 doped samples show an increase in the impedance with temperature. The increase is related to the extent of dopant concentration. Moreover the rate of the decrease in the impedance is higher for high concentration of I_2 .

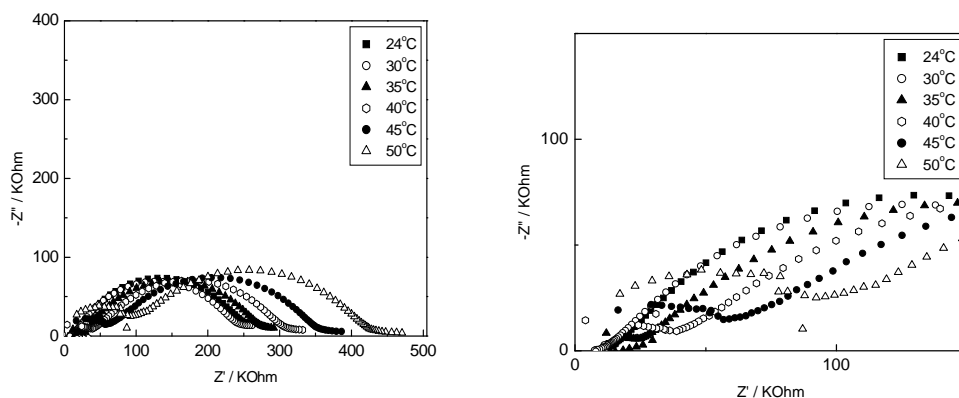


Figure 1. Temperature effect on the impedance behavior of SS / $Li_2Pc:I_2$ (95:5) / SS

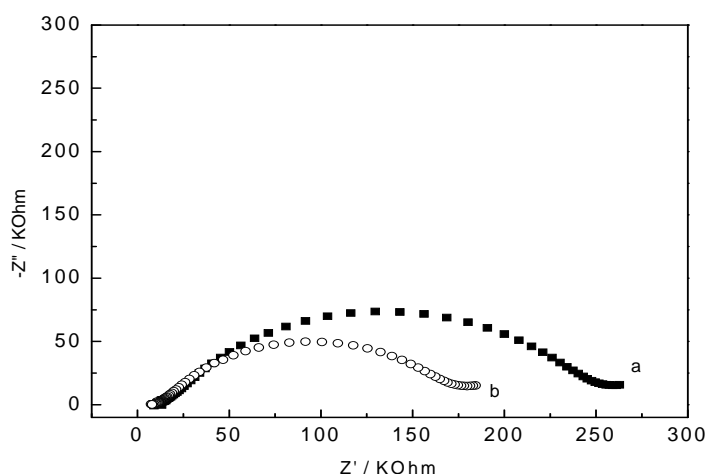


Figure 2. Nyquist plot (a) at room temperature before heating experiments (b) at room temperature after heating the cell to 70°C followed by cooling.

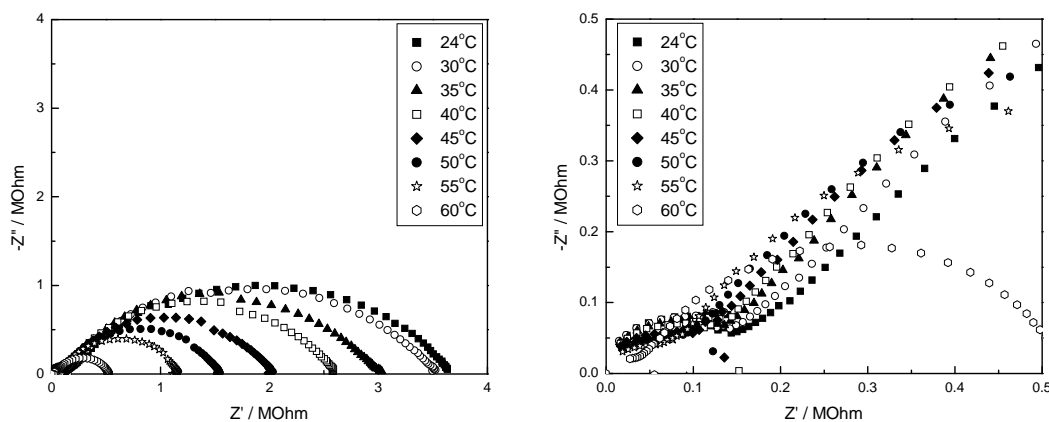


Figure 3. Impedance plots of undoped $\text{Li}_2\text{Pc SS/Li}_2\text{PC/PVDF/SS}$ cell

Temperature dependent impedance measurements were carried out immediately after assembling the cells. The thermal fluctuation might be suppressing the long range order in the system. Figure 4 shows an increase in impedance; this shows clearly that I_2 plays an important role in affecting the long range order in the system and in the intermolecular charge transport.

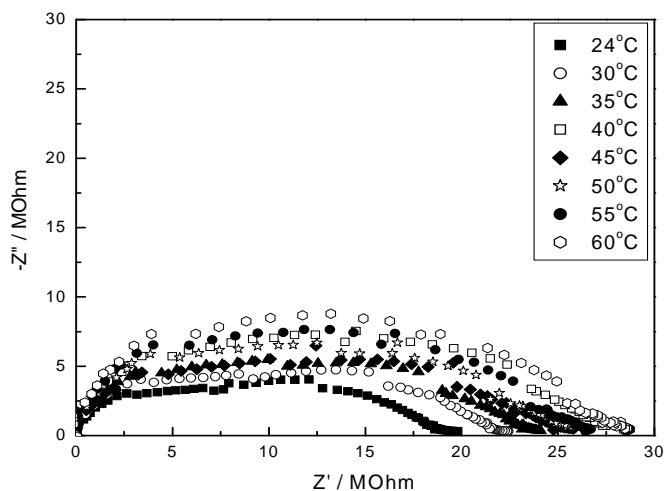


Figure 4. Cell - SS/Li₂Pc:I₂ (95:5)/SS Temperature effect on the impedance behavior immediately after assembling

Time dependent impedance of this solid state doped system shows a gradual decrease in the impedance (Fig. 5). From figure 5, it is clear the total impedance decreases by about ten times after 278 hr of assembly. It is also observed that the initial impedance for higher concentration of I₂ is higher in comparison with low concentration of Iodine.

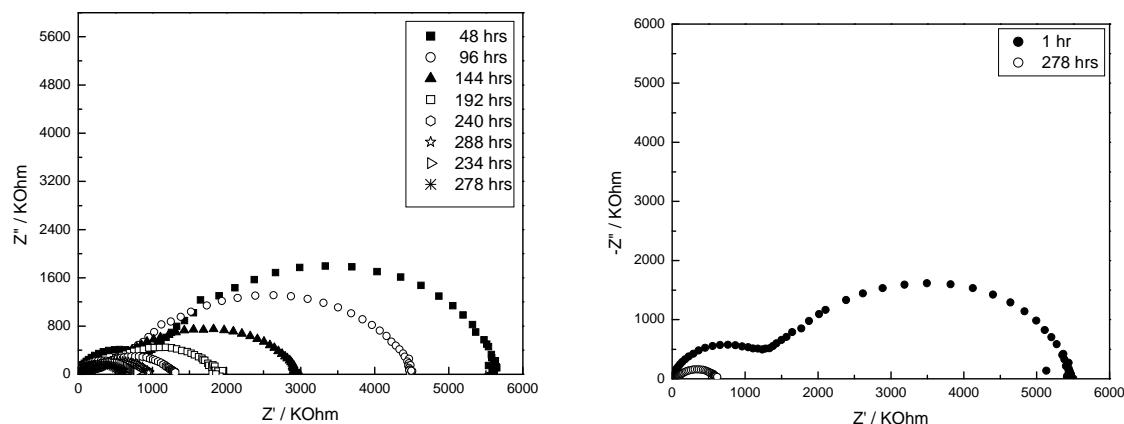


Figure 5. Time dependent impedance plot of cell SS/Li₂Pc:I₂ (95:5)/ SS

DC bias voltage dependent impedance measurements were done with Li₂Pc:I₂ of 95:5 which shows an interesting behaviour unlike that of the undoped system. Only with Li₂Pc, in the DC bias dependent experiments, there is a decrease in the second semicircle impedance and nearly constant first semicircle impedance was observed with all the voltages (0 to 4 V). But in the case of all I₂ doped system the 2nd semicircle decreases with applied DC voltage, while the 1st semicircle impedance starts increasing beyond

0.75 V or 1 V. Figure 6 shows the impedance plot of 5% iodine doped system at different DC bias voltages.

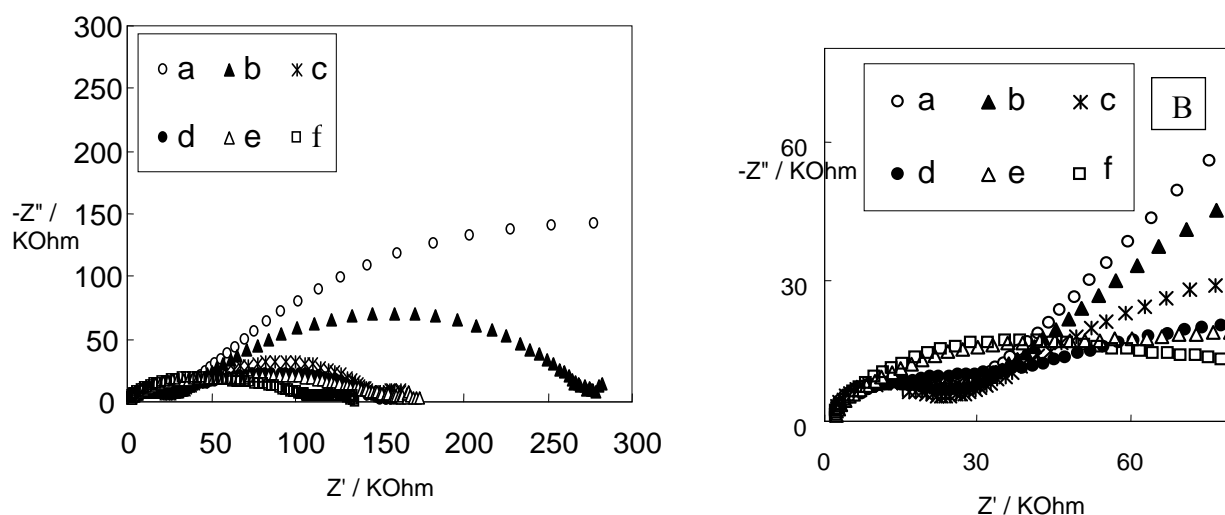


Fig.6 Nyquist plot of the SS/Li₂Pc:I₂(95:5)/SS under different DC bias voltage conditions a – 0 V, b – 0.25 V, c – 0.5 V, d – 1 V, e – 1.5 V, f – 2 V, (B) high frequency region expanded.

In the infrared spectra the intensity of band centered at 1600 cm^{-1} is increased after I₂ doping with the band width is of 100 cm^{-1} . This is due to reduction of electron density in the ring system. It is also clearly indicated by the shift in the 1600 cm^{-1} band to 1594 cm^{-1} (after 1 day) and to 1584 cm^{-1} (after 4 days). Also a band at 1484 cm^{-1} disappears in the I₂ doped system. The IR band at $888\text{-}919 \text{ cm}^{-1}$ is assigned for M-N bond

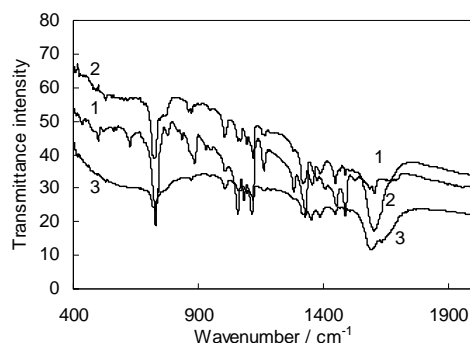


Figure 7. Infrared spectra of (1) Li₂Pc undoped, (2) 10 % I₂ doped (after 1 days), (3) 10 % I₂ doped (after 4 days).

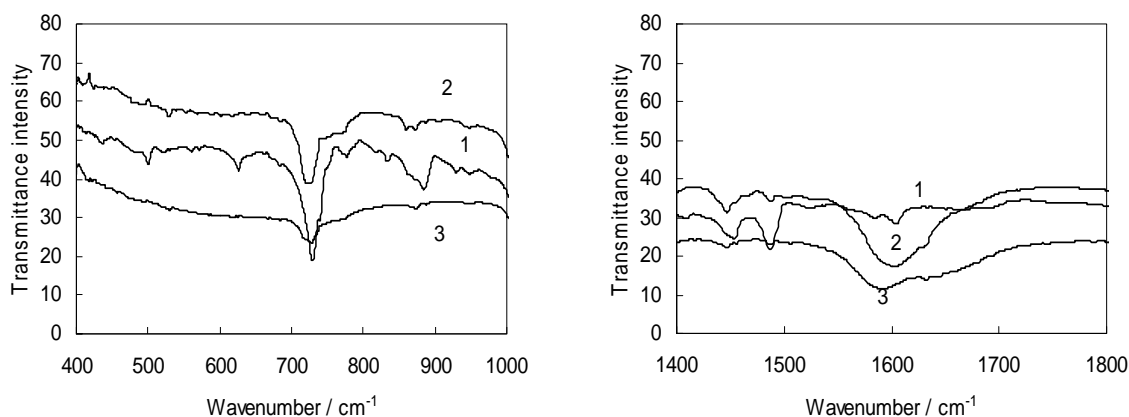


Figure 7(b). Expanded region of infrared spectra of (1) Li_2Pc undoped, (2) 10 % I_2 doped (after 1 days), (3) 10 % I_2 doped (after 4 days).

vibration (Fig. 7). In Li_2Pc it is at 880 cm^{-1} which starts to decrease in the intensity with I_2 doping level (Fig. 8). Band at 728 cm^{-1} attributed to M-N out of bending mode vibration, decreases in the peak intensity. Also peak at 1278 cm^{-1} assigned for M-N vibrational frequency shows a decrease in the intensity. The effect of I_2 is reflected in UV-Vis spectra (Fig. 8) also.

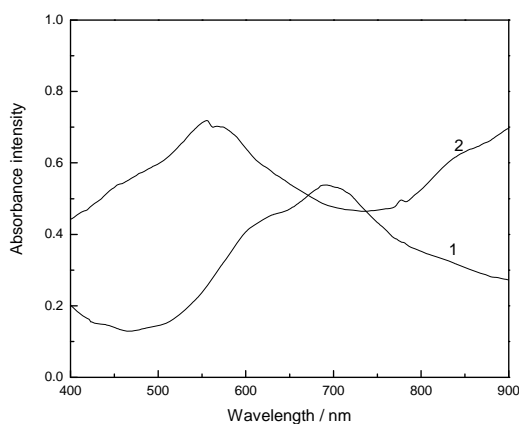


Figure 8. UV-Vis of 10 % doped (curve 1) and undoped (curve 2) Li_2PC grounded with KBr as pellet.

XRD pattern (Fig. 9) of Li_2PC doped with 10% I_2 shows the 100% intensity peak at $2\theta = 69^\circ$ which corresponds to the α form of Li_2Pc . Also peak broadening was

observed compared to that of undoped Li_2Pc . In the I_2 doped sample, peaks at 2θ values 11.3, 16.4, 17.25, 19.2, 22.7° were not observed. In addition the peaks at 14, 21.35 intensity are lowered and broadened in comparison with that of undoped Li_2Pc .

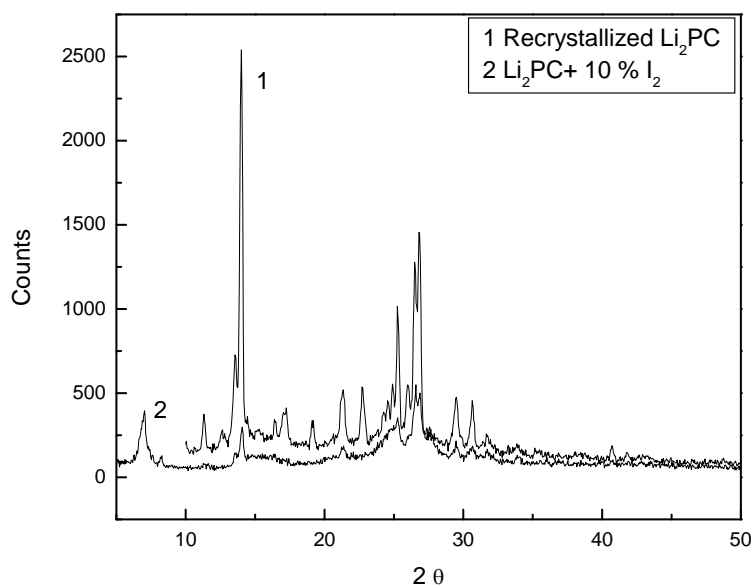


Figure 9. XRD patterns of 1 - Li_2PC recrystallized, 2- 10% I_2 doped Li_2Pc powder after 10 days. Initially the sample was grounded and kept as a solid pellet.

4. Thin film of dilithium phthalocyanine impregnated Celgard membrane

The pellets of Li_2Pc exhibit very high values of impedance. It was intended to decrease thickness for obtaining lower impedance. Some approaches are listed below:

(i) Coating of Li_2Pc on Celgard membrane:

15 mg of Li_2PC was spread evenly on both sides of the porous polypropylene Celgard membrane and pressed for 5 mins at 50 KN. Then it was used as an electrolyte between two symmetrical stainless steel electrodes for impedance measurements (Fig. 1). The impedance is still high due to insulating Celgard membrane.

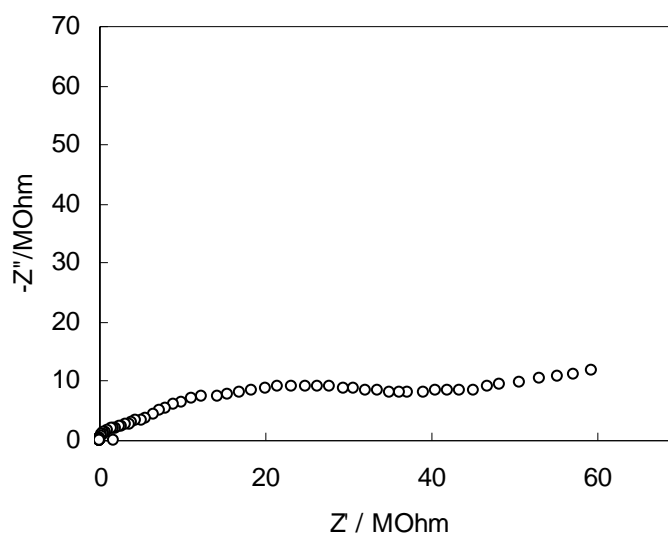


Figure 1. Nyquist plot of SS/ Li_2PC on cell guard membrane /SS at room temperature.

A Celgard membrane was soaked in Li_2Pc dissolved in DMF and dried. The pores of the membrane was expected to be filled with Li_2Pc . This was used for impedance measurement. It also showed very high impedance and steep spike in the Nyquist plot. There was no semicircle.

(ii) Coating of Li_2Pc on stainless steel:

Li_2Pc with 5 weight percent of PVDF was made as slurry and coated on SS electrode as thin film, and dried at 45°C under vacuum. Impedance was measured by combining it with another SS electrode (Fig. 2). The impedance obtained is lower than the impedance of Li_2Pc pellets.

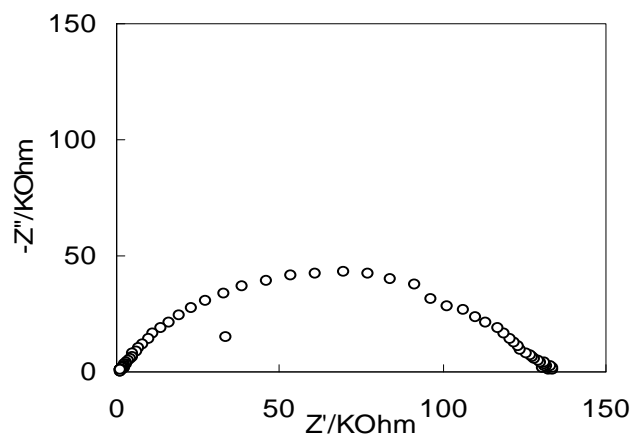


Figure 2. Nyquist plot of SS/ Li_2Pc +PVDF+NMP (thin film)/SS cell

The time dependant experiments showed an increase in impedance with increase in time after cell assembly (Fig. 3).

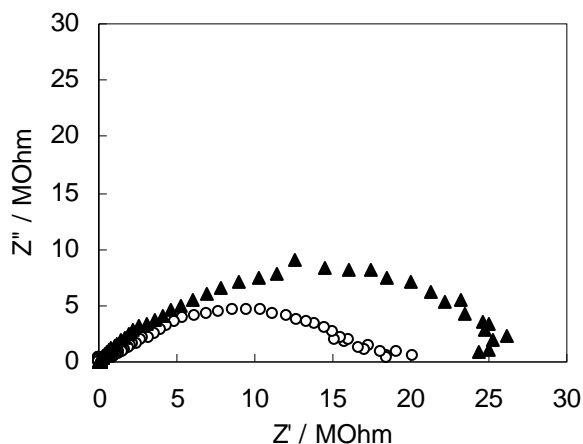


Figure 3 – Time dependent impedance behavior of SS/Li/ Li_2Pc +PVDF/SS

o (1 hr), Δ (24 hrs).

(iii) Impedance of LiPc:

LiPc was prepared by electrochemical oxidation of Li_2Pc (0.01 M) dissolved in acetonitrile containing TBAP (0.1 M) using potentiodynamic methods. The insoluble powder collected at the bottom of the cell was washed with acetonitrile and dried at 45°C in vacuum. This powder was made as pellet and the cell SS /LiPc / SS was assembled. Figure 4 shows the Nyquist plot the cell at room temperature.

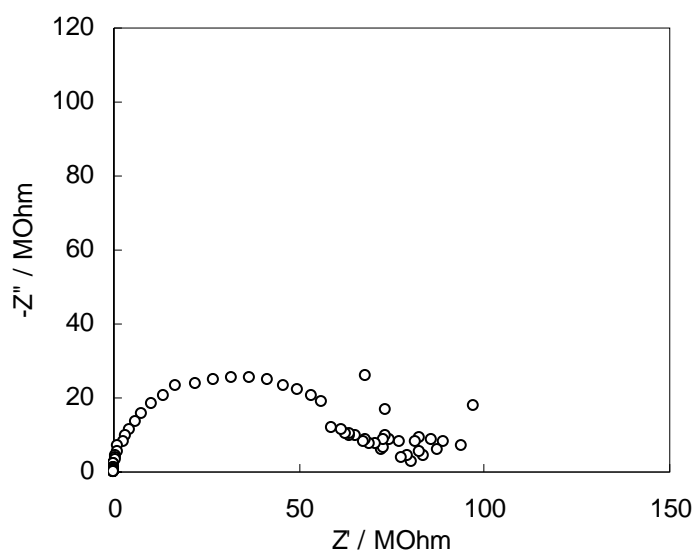


Figure 4. Nyquist plot of SS /LiPc (electrooxidised) / SS

5. Impedance of dilithium phthalocyanine in contact with different metallic substrates

In this study, different metal substrates were used as electrodes to measure the impedance characteristics of Li_2Pc pellets. It is reported that in metal-semiconductor interface, conductivity will not be bulk limited if the semiconductor thickness is small. The thickness of the semiconductor and the work function of the electrode decide the bulk conductivity. Considerable variation of conductivity with applied voltages is expected. If a metal forms the blocking contact (electronic) on the electrode surface there is a transition from electrode limited conductivity to bulk limited conductivity. The barrier height depends on the thickness of the film present on the surface. In these systems, bulk characteristic is dominant at lower applied voltages.

In the present experiment, different electrode materials, namely SS, Au foil, Au foil sputtered on SS, Cu, Ni, Al and Li were used to measure the impedance of Li_2Pc . Recrystallized Li_2Pc was pressed in the form of a pellet (12 mm diameter) using 25 mg of fine powder under 25 KN pressure. The impedance of SS/ Li_2Pc /SS cell (Fig. 1) consists of two semicircles as described in Section 1 of this report. Nyquist plots of impedance under different values of DC bias voltages are also similar to Fig. 4 on page 14 of section 1. There is a decrease in diameter of the low frequency semicircle with increase of voltage. The high frequency semicircle is nearly constant. The impedance of Au/ Li_2Pc /Au cell without dc bias voltage is shown in Fig. 2. This data differ from the data of SS/ Li_2Pc /SS cell. Now there is only a single semicircle and its impedance is considerably lower than the SS/ Li_2Pc /SS cell. Furthermore, the impedance data recorded by applying different dc bias voltages (Fig. 3) indicate that the data are nearly the same at all voltages. A comparison of the data of SS/ Li_2Pc /SS cell (Fig. 1) and Au/ Li_2Pc /Au cell (Figs. 2 and 3) suggests that the interfacial resistance at metal/ Li_2Pc interface plays an important role in the magnitude of impedance as well as its nature. Similar to the Au foil, the impedance data of Li_2Pc measured between Au sputtered on SS consist of a single semicircle with low value of impedance (Fig. 4). The impedance spectrum of Cu/ Li_2Pc /Cu exhibits elongated, broad semicircle suggesting overlap of two semicircles (Fig. 5). The diameter of the broad semicircle decreases substantially with an increase in dc bias voltage (Fig. 6). The impedance spectrum of Ni/ Li_2Pc /Ni cell is shown in Fig. 7. There is only a single semicircle. The spectrum of Al/ Li_2Pc /Al (Fig. 8) shows a

semicircle with a high value of impedance. However, the cell impedance decreases significantly if Al is etched in dil. HCl to remove the surface oxide film before the cell assembly (Fig. 9). The spectrum of Li/ Li₂Pc/Li is an elongated semicircle (Fig. 10).

The above studies suggest two contributory factors for various of impedance of Li₂Pc when measured using different metals. One factor is the surface resistance of the metal and the other is the chemical reactivity of Li₂Pc with the metal.

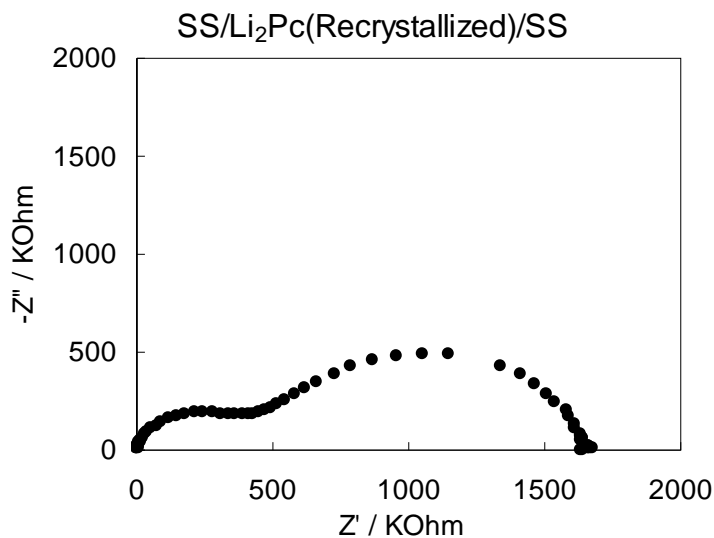


Fig. 1. Nyquist plot of SS/Li₂Pc/SS cell

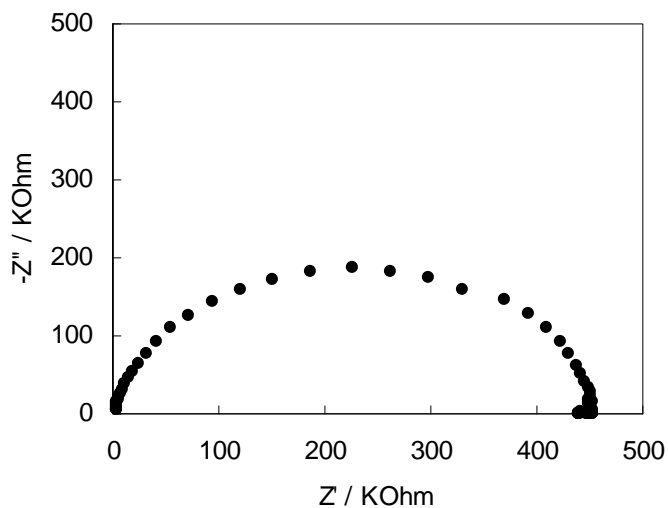


Fig. 2. Nyquist plot of Au/Li₂Pc/Au at room temperature

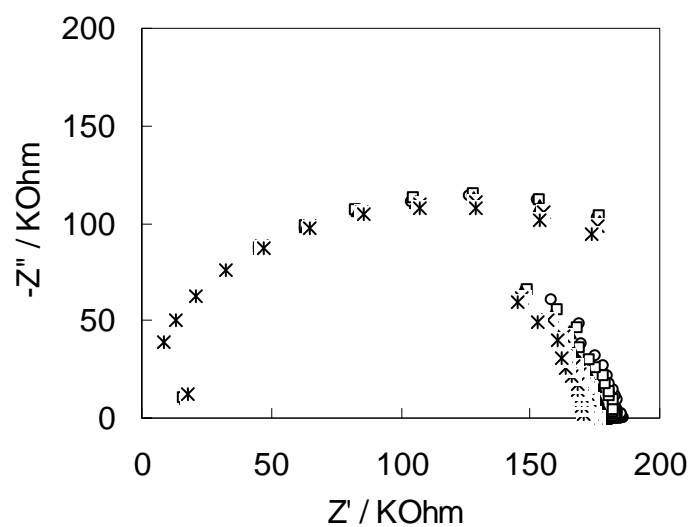


Fig. 3. Au/Li₂Pc/Au – DC Bias Voltage dependent impedance behaviour
 o – 0 V, □ - 0.25 V, ▲ - 0.5 V, × - 0.75 V, * - 1 V

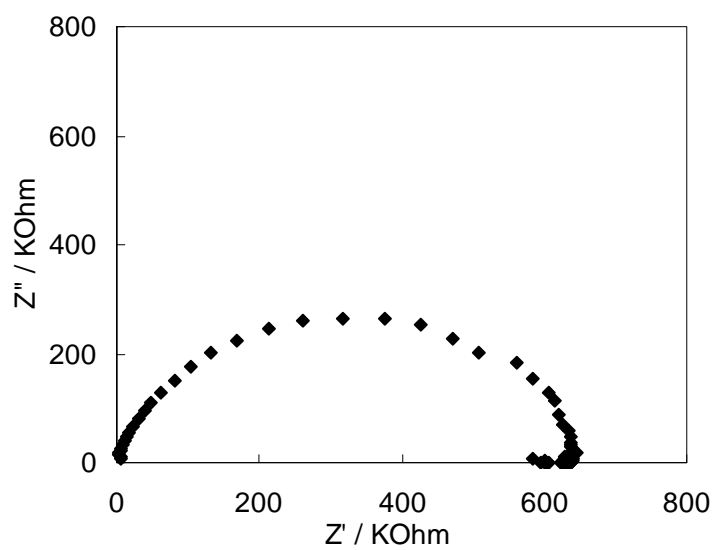


Fig. 4. Nyquist plot of SS/Au (sputtered)/Li₂PC/Au (sputtered)/SS

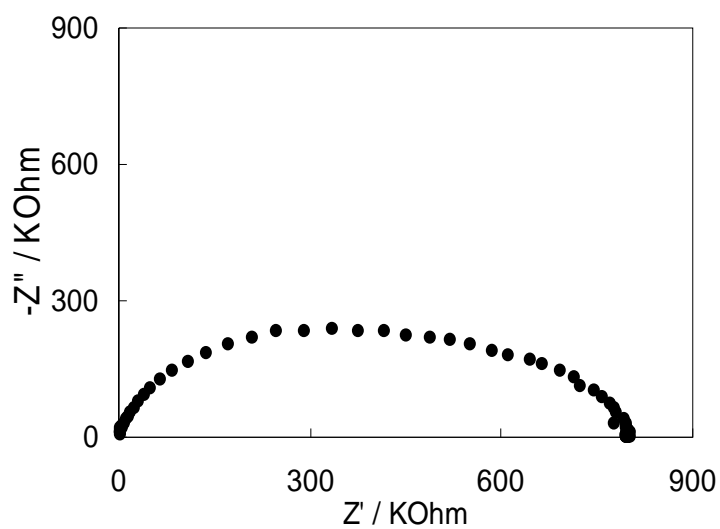


Fig. 5. Nyquist plot of SS/Cu/Li₂Pc/Cu/SS at room temperature and at OCV

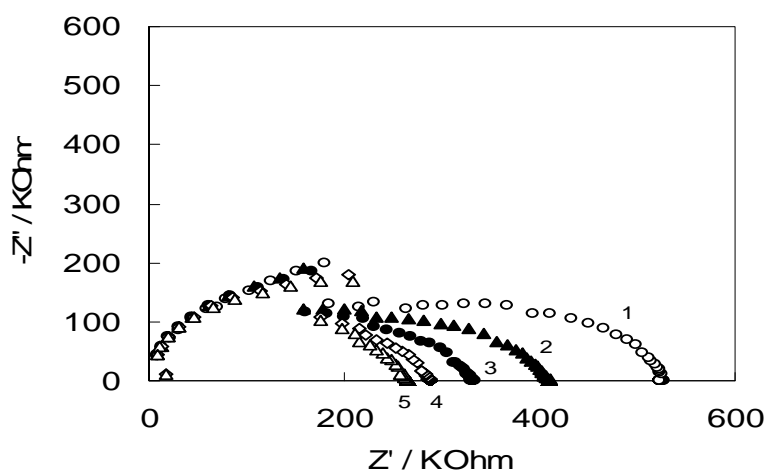


Fig. 6. DC Bias voltage dependent impedance behaviour of Cu/Li₂Pc/Cu cell. 1 – Open Circuit Voltage 0 V, 2 – 0.25 V, 3 – 0.5 V, 4 – 0.75 V, 5 – 1 V

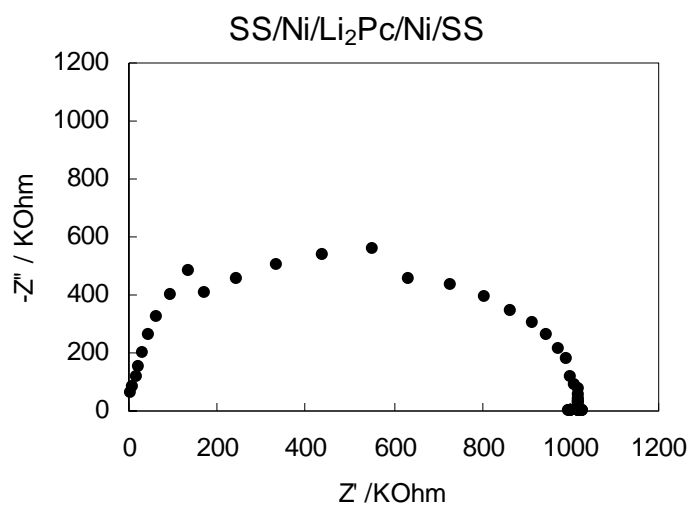


Fig. 7

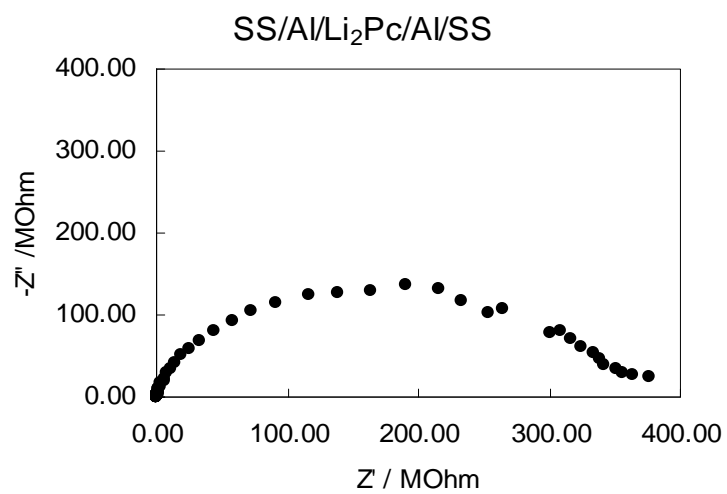


Fig. 8

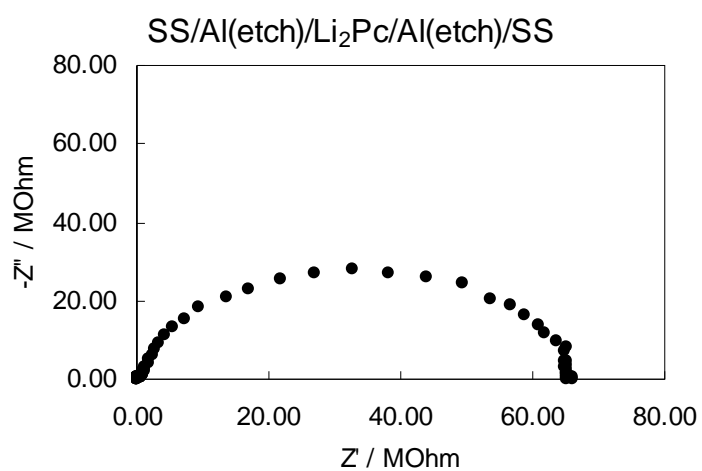


Fig. 9

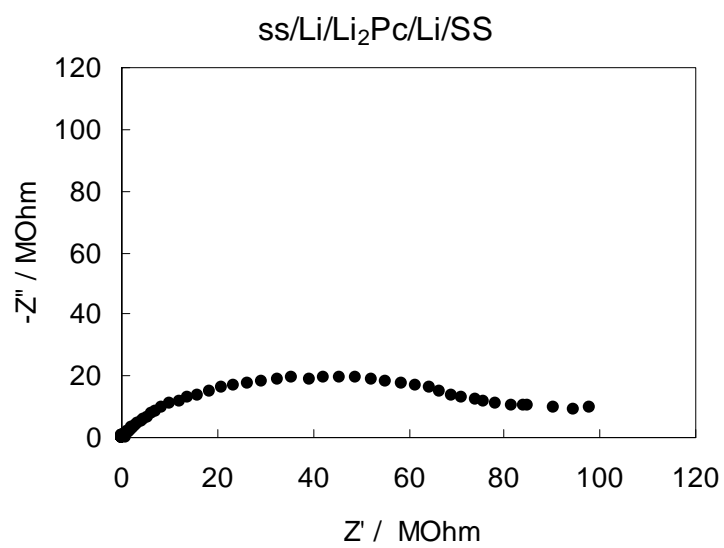


Fig. 10

6. Capacitance studies of dilithium phthalocyanine and lithium phthalocyanine

Electrodeposited LiPc on stainless steel (SS) electrode were subjected to capacitance measurement in non-aqueous and aqueous electrolytes. Electrodeposition of LiPc was carried out by potentiodynamic experiments at a scan rates of 20 mV/s. The weight of the material obtained was in the range of 0.2 to 0.6 mg/cm². Figure 1 shows cyclic voltammograms of LiPc coated SS electrode in DMSO containing 0.2 M LiBF₄. Here cyclic voltammograms were recorded with different potential ranges. Cyclic voltammograms shows a steep increase in current beyond 1 V with respect to Ag /AgCl reference electrode. The charge-discharge measurements were carried out different current densities and in different voltage ranges. When the potential increased to 1.3 V there is slight nonlinearity observed in the charging curve, which is also seen in CV. The specific capacitance values obtained is given in the corresponding figures.

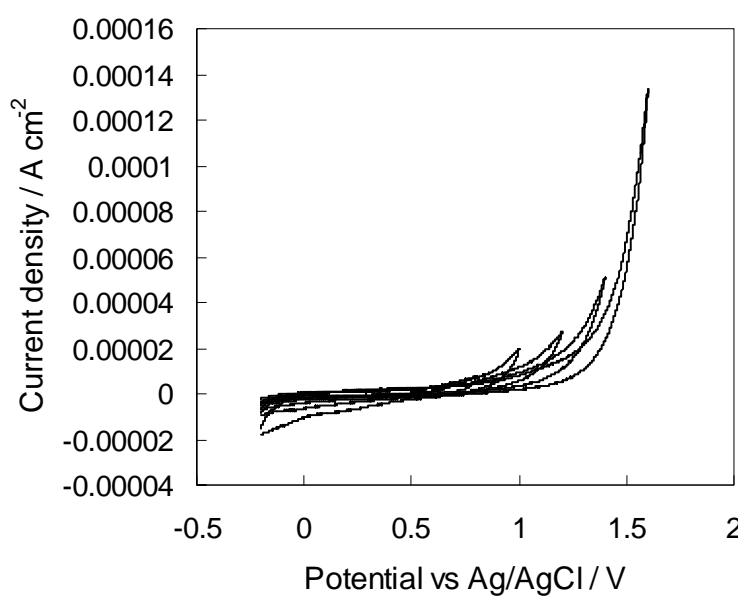


Figure 1 - Cyclic voltammograms of SS/LiPc electrode with different potential range in DMSO + 0.1 M LiBF₄ (scan rate 20 mV/s).

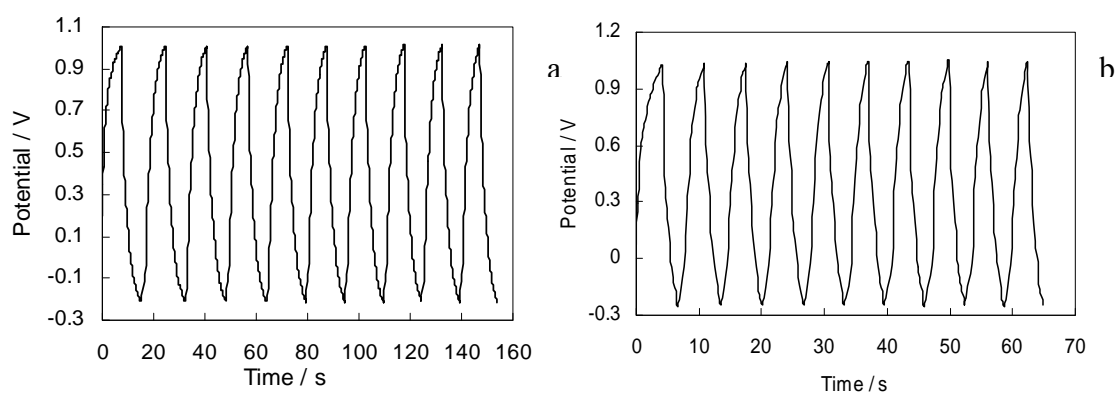


Figure 2 - Charge-discharge cycles of LiPc/SS electrode in DMSO + 0.1 M LiBF₄ at different current densities. (a) 0.363 F/g (10 $\mu\text{A}/\text{cm}^2$) and (b) 0.196 F/g (20 $\mu\text{A}/\text{cm}^2$)

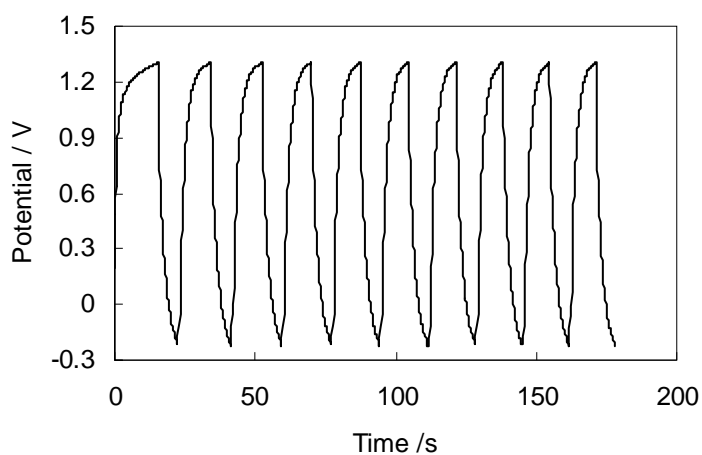


Figure 3 - Charge discharge curve for SS / LiPc electrode with higher potential range. Specific capacitance = 0.424 F/g,

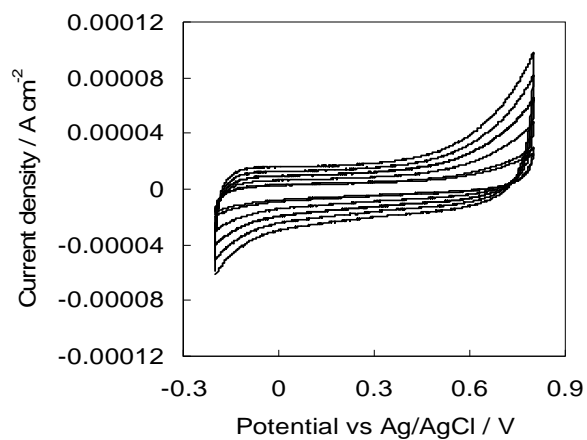


Figure 4. LiPc / SS electrode in 0.1 M Na_2SO_4 at different scanrates, 5 to 200 mV/s

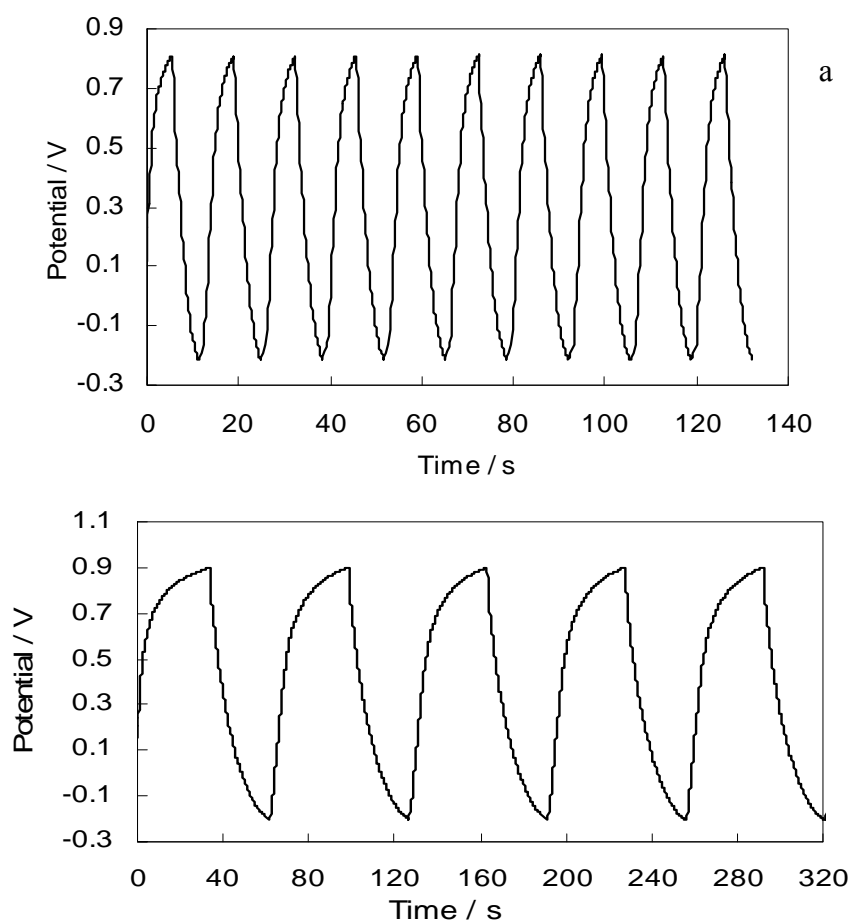


Figure 5 - Charge discharge cycles of LiPc / SS electrode in 0.1 M Na_2SO_4 at (a) $20 \mu\text{A} / \text{cm}^2$ (0.709 F/g and (b) $10 \mu\text{A} / \text{cm}^2$ (1.54 F/g).

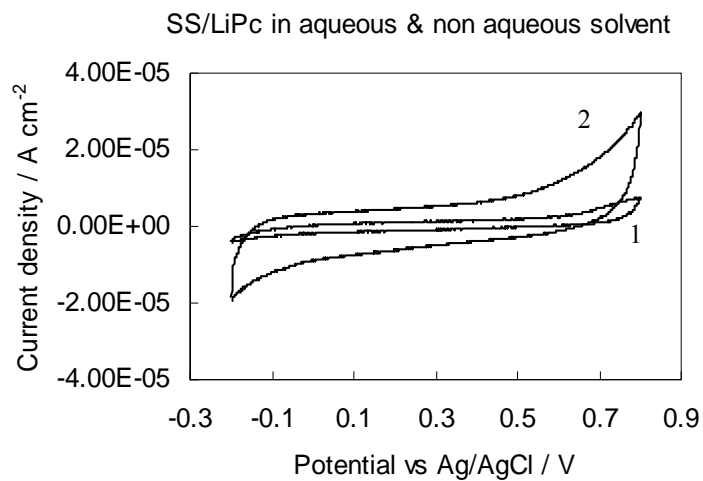


Figure 6 - Cyclic voltammograms of LiPc / SS electrode – (1) in DMSO + 0.1 M LiBF₄ and (2) in 0.1 M Na₂SO₄. Scan rate : 20 mV / s.

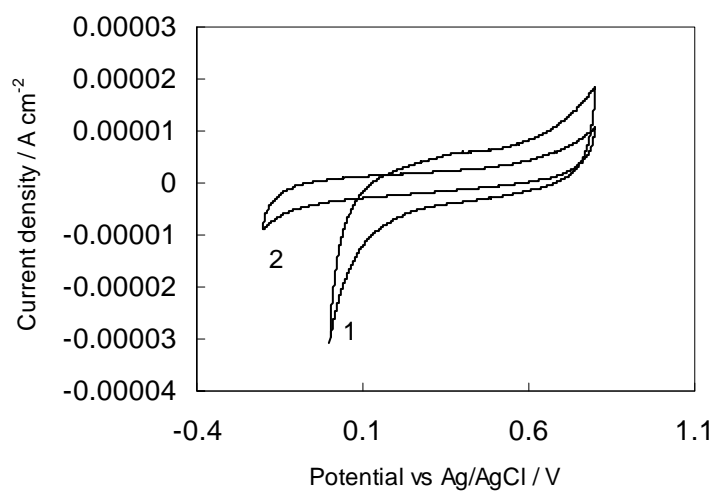


Figure 7 - Cyclic voltammograms of LiPc / Pt (1) and LiPc/SS (2) electrodes in 0.1 M Na₂SO₄ at 20 mV / s. LiPc was electrodeposited potentiodynamically for 10 cycles.

Stainless steel and platinum electrode was coated with a slurry made from Li_2Pc + PVDF (5 weight percent) and dried in vacuum at 45°C . These electrodes were used for capacitance measurements in aqueous and non aqueous electrolytes. Here the potential window was low when compared to LiPc coated electrodes. The H_2SO_4 treated electrodes exhibited relatively higher capacitance values in the non aqueous electrolyte. Highest specific capacitance value of 1.54 F/g is obtained in aqueous electrolyte with Li_2Pc coated on platinum electrode. The value of specific capacitance obtained with SS / LiPc electrode is higher to that of $\text{Li}_2\text{Pc} / \text{SS}$.

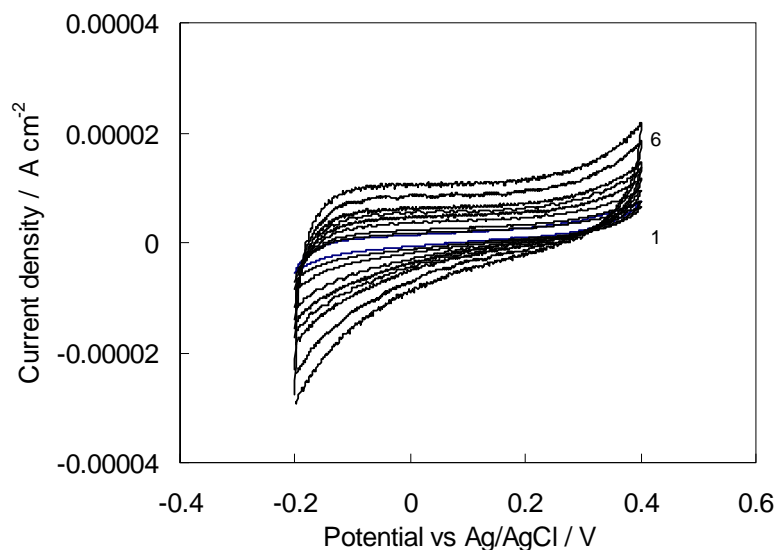


Figure 8 - Cyclic voltammograms of stainless steel electrode (0.5 cm^2) coated with 0.4 mg of $\text{Li}_2\text{Pc}+\text{PVDF}+\text{NMP}$ at different scan rates in $0.1 \text{ M Na}_2\text{SO}_4$. 1 – 5 mV/s , 2- 20 mV/s , 3- 60 mV/s , 4 – 100 mV/s , 5 – 150 mV/s and 6- 200 mV/s .

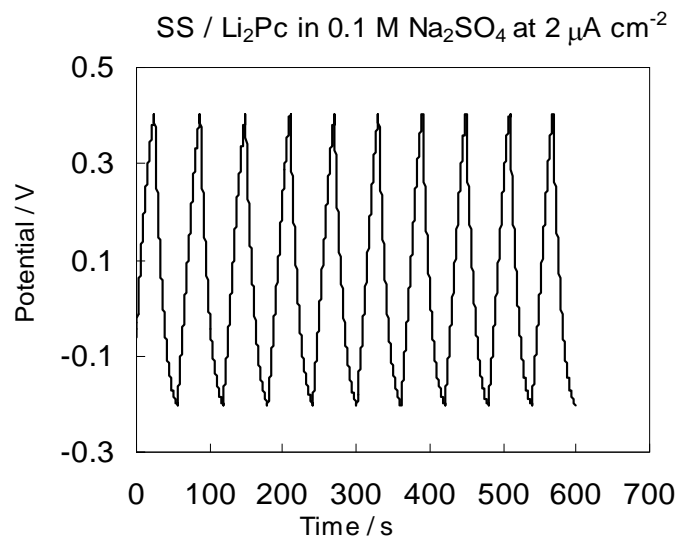


Figure 9 - Charge discharge cycles of stainless steel electrode coated with $\text{Li}_2\text{Pc} + \text{NMP}$ in $0.1 \text{ M Na}_2\text{SO}_4$ at $2 \mu\text{A} / \text{cm}^2$. Capacitance = 0.139 F/g .

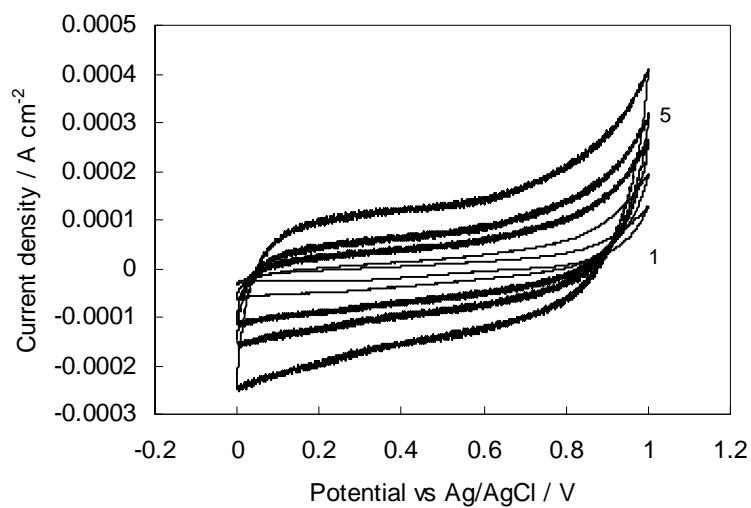


Figure 10 - Cyclic voltammograms of LiPc/Ptin DMSO + 0.1 M LiBF_4 , after dipping in $0.05 \text{ M H}_2\text{SO}_4$, followed by washing with DD water and DMSO. The electrode was kept in DMSO for 1 hr before recording the CV at different scan rates.

Figure 11 - Cyclic voltammograms of LiPc / SS in 0.1 M Na₂SO₄, at different scan rates 5 mV/s to 200 mV/s

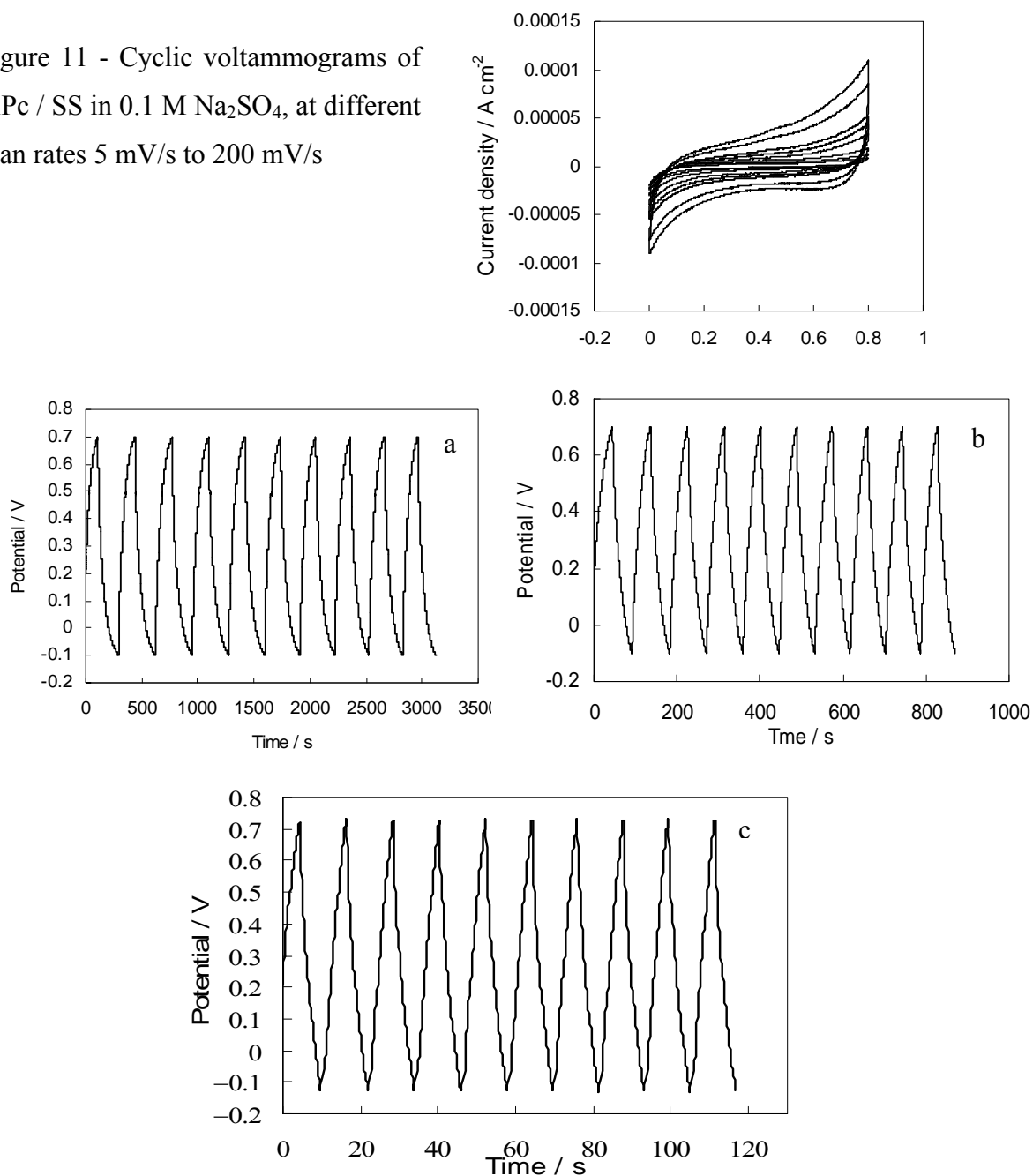


Figure 12. Charge-discharge cycles of LiPc/Pt electrode treated with 0.05 M H₂SO₄, in DMSO + 0.1M LiBF₄ at different current densities. (a) 10 μ A / cm² - 1.59 F/g , (b) 20 μ A / cm² - 0.982 F/g , (c) 100 μ A / cm² - 0.711 F/g.

7. Dilithium phthalocyanine as a cathode material

(A) Studies of Li_2Pc as the cathode material in non-aqueous liquid electrolyte medium

Since Li_2Pc is a mixed ionic and electronic conductor, and some metal phthalocyanines are studied as cathode materials, it is intended to study the properties of Li_2Pc as the cathode material. For this purpose, several electrodes are prepared and characterized in liquid electrolytes by combining with lithium metal as the anode. Electrodes are prepared on aluminium substrates. Aluminium (flag-shape) strip (flag area = 0.6 cm^2) was sectioned out of a sheet of thickness 0.5 mm, and it was polished, washed and dried in vacuum at ambient temperature. A slurry of Li_2Pc (recrystallised) + acetylene black + PVDF (weight ratio: 47:47:6) was mixed thoroughly in NMP, and applied onto the pre-treated Al flag. The coated electrode was dried at 100°C in vacuum to remove the solvent and transferred to argon filled glove box (MBraun, model UNILAB). A mixed solvent of ethylene carbonate and dimethyl carbonate containing 1M LiBF_4 was used as the electrolyte. Cells were assembled in glass containers using lithium as the anode. The open-circuit voltage of the cell was 3.564 V. The cell was discharged at $100 \mu\text{A}/\text{cm}^2$ to 2.0 V. The variation of cell voltage with time of discharge is shown in Fig. 1. A discharge capacity of 127 mAh/g was obtained. It was found that the electrolyte turned yellow in color after the discharge. The cell was subjected to charging at $100 \mu\text{A}/\text{cm}^2$ till cell voltage reached 4.0 V (Fig. 2). It was found that the charging capacity was only 17 mAh/g. The discharge capacity and charge capacity during the second cycle were 60 mAh/g and 14 mAh/g, respectively. Thus, there was a considerable decrease in capacity, suggesting poor cyclability of Li_2Pc . Furthermore, it was found the yellow colour of the electrolyte became more intense, probably due to slow dissolution of the active material from the electrode. Another cell was assembled to check the reproducibility of the above results. Discharge and charge curves are shown in Figs. 3 and 4, respectively. The electrolyte turned into yellow colour and it was concluded that Li_2Pc was not stable in the electrolyte. Furthermore, the ac impedance data showed (Fig. 5) that the cell impedance increases after subjecting the cell to a charge-discharge cycle.

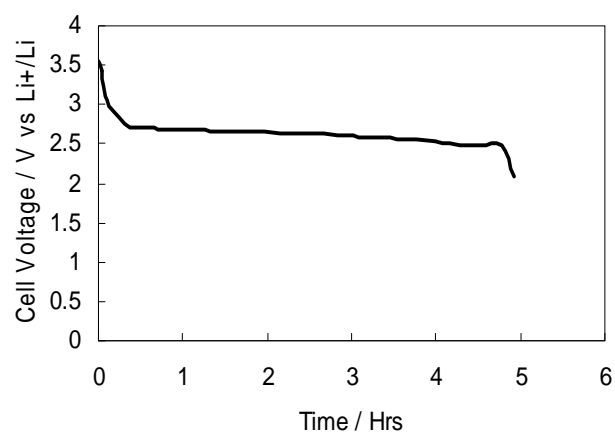


Figure 1. Discharge curve of Li/Li₂Pc cell in non-aqueous electrolyte

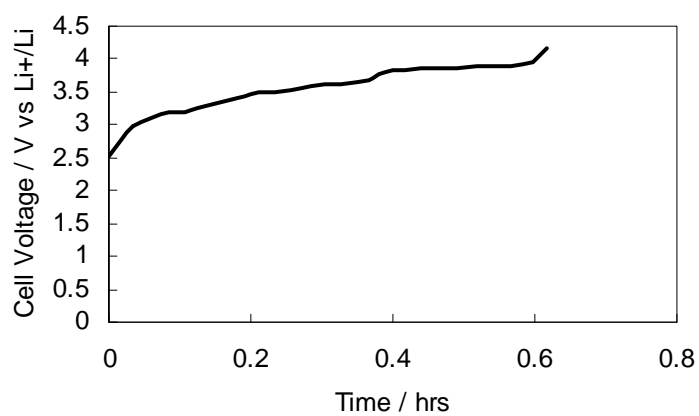


Figure 2. Charging curve of Li/Li₂Pc cell in non-aqueous electrolyte

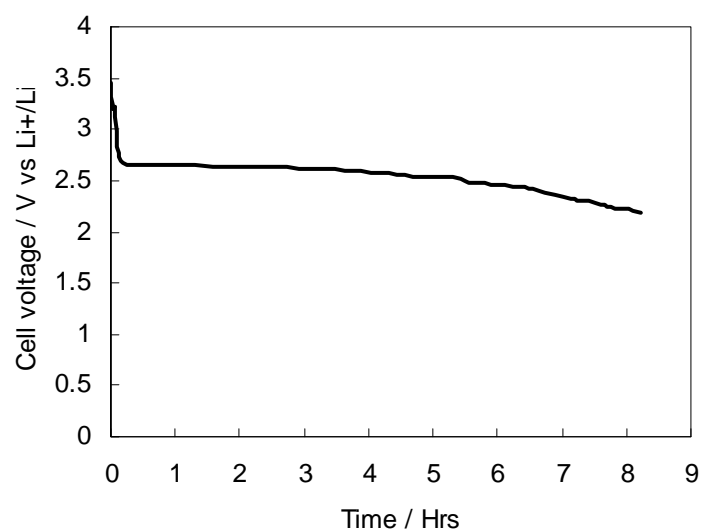


Figure 3. Discharge curve of a Li/Li₂Pc cell in non-aqueous electrolyte

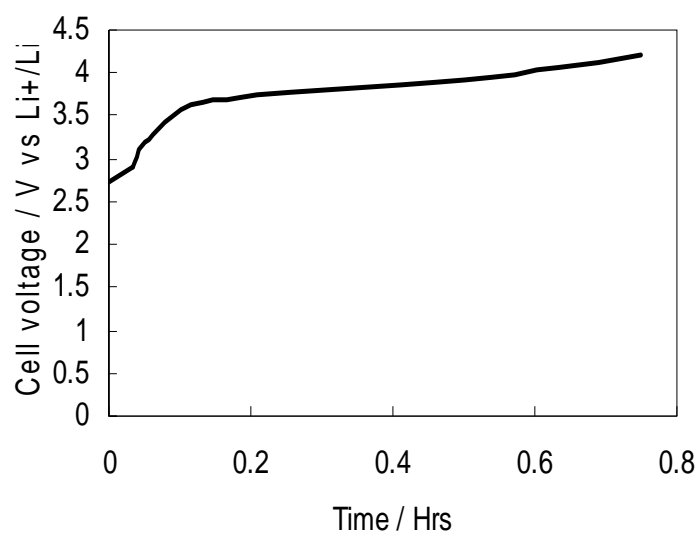


Figure 4. Charging curve of a Li/Li₂Pc cell in non-aqueous electrolyte

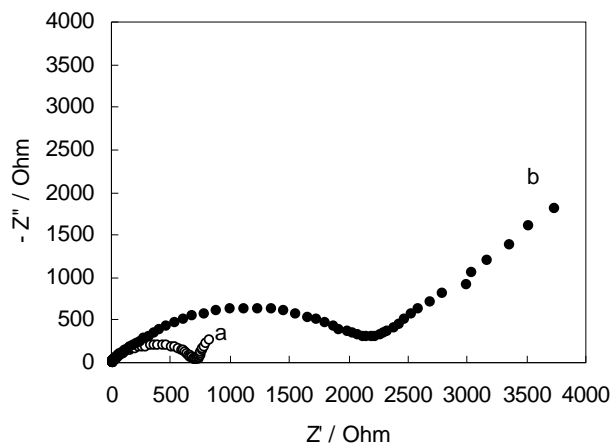


Figure 5. Nyquist impedance plot of a Li/Li₂Pc cell in non-aqueous electrolyte, (a) before and (b) after a charge/discharge cycle.

(B) Studies of Li₂Pc as the cathode material in gel polymer electrolyte medium

Because of solubility of Li₂Pc in liquid organic electrolyte as described above, it was attempted to characterize Li₂Pc as cathode material in gel polymer electrolyte (GPE) medium. A GPE film was prepared by heating a suspension of 1g Polymethylmethacrylate, 2.5g ethylene carbonate, 2.5g propylene carbonate and 0.4g LiBF₄ at 80°C in nitrogen atmosphere. The conductivity of GPE was measured by sandwiching between SS electrodes. The ambient temperature conductivity is 1.1×10^{-3} S/cm; and the temperature dependant conductivity follows Arrhenius relationship as shown in Fig. 6. Li/GPE/Li₂Pc cells were assembled in argon atmosphere glove box and subjected to charge-discharge cycling. The first charge-discharge curves at a current density of $64 \mu\text{A}/\text{cm}^2$ are shown in Fig. 7. A capacity of 80 mAh/g is obtained during discharge. The current density was decreased to $32 \mu\text{A}/\text{cm}^2$ in the subsequent cycles. The charge-discharge curves of the second cycle are shown in Fig. 8, and variation of

discharge capacity with cycle number in Fig. 9. The capacity decreases from about 90 mAh/g to 40 mAh/g in 6 charge-discharge cycles. Although the performance of Li_2Pc is better in GPE medium than in non-aqueous liquid electrolyte, the decrease in capacity on repletion of charge-discharge cycling reflects poor rechargeability of Li_2Pc . AC impedance measurements of the $\text{Li}/\text{GPE}/\text{Li}_2\text{Pc}$ were performed after charging of each cycle and the impedance was found to increase with cycle number (Fig. 10), thus, in agreement with the discharge capacity data. Another cell- $\text{Li}/\text{GPE}/\text{Li}_2\text{Pc}$ was assembled to check the reproducibility of the data. The charge-discharge data are presented in Figs. 11-12, and the cycle-life data in Fig. 15. The capacity of this cell also decreases rapidly of cycling. The next cell in this series was assembled with a Li_2Pc electrode of loading level of 0.15 mg/cm^2 , against 2.0 mg/cm^2 of the previous $\text{Li}/\text{GPE}/\text{Li}_2\text{Pc}$ cells. The charge-discharge data and cycle-life data are presented in Figs. 16 and 17, respectively. Although the discharge capacity of the first cycle is higher than that of higher loading level cell, the capacity decreases with cycle number, in this case also. Similar data of another $\text{Li}/\text{GPE}/\text{Li}_2\text{Pc}$ are shown in Figs. 18 and 19.

It is concluded from the above studies that Li_2Pc behaves as a cathode material, but with poor rechargeability. Perhaps this compound is more suitable for primary battery application than secondary battery application.

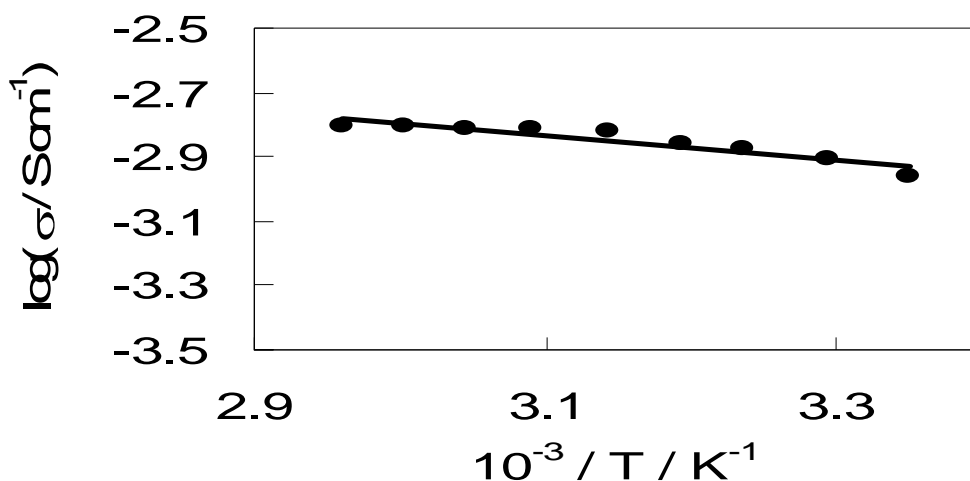


Figure 6. Arrhenius plot of gel polymer electrolyte.

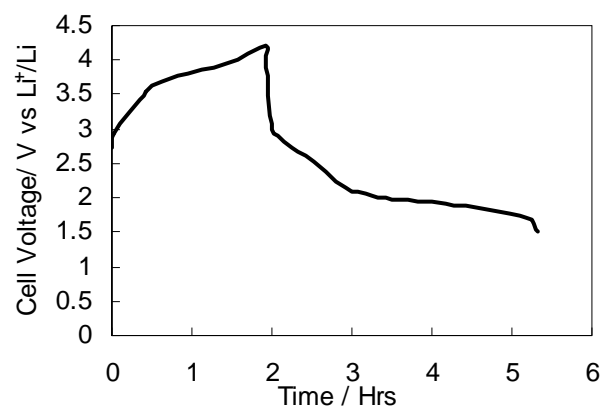


Figure 7. Charge-discharge curves of a Li/GPE/Li₂Pc cell at a current density of 64 $\mu\text{A}/\text{cm}^2$

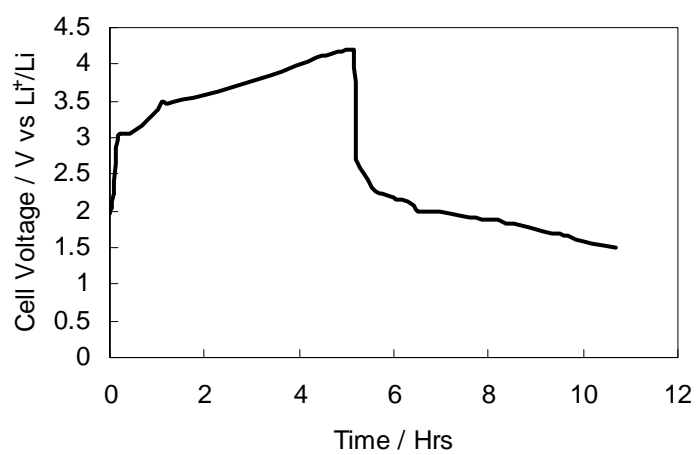


Figure 8. Charge-discharge curves of a Li/GPE/Li₂Pc cell at a current density of 32 $\mu\text{A}/\text{cm}^2$

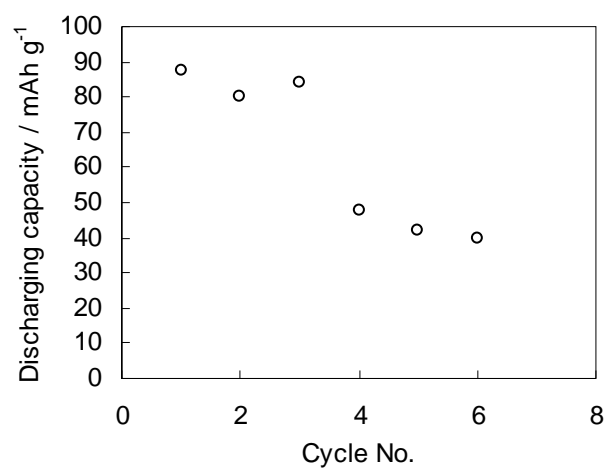


Figure 9. Variation of capacity of a Li/GPE/Li₂Pc cell with cycle number. Current density: 32 $\mu\text{A}/\text{cm}^2$

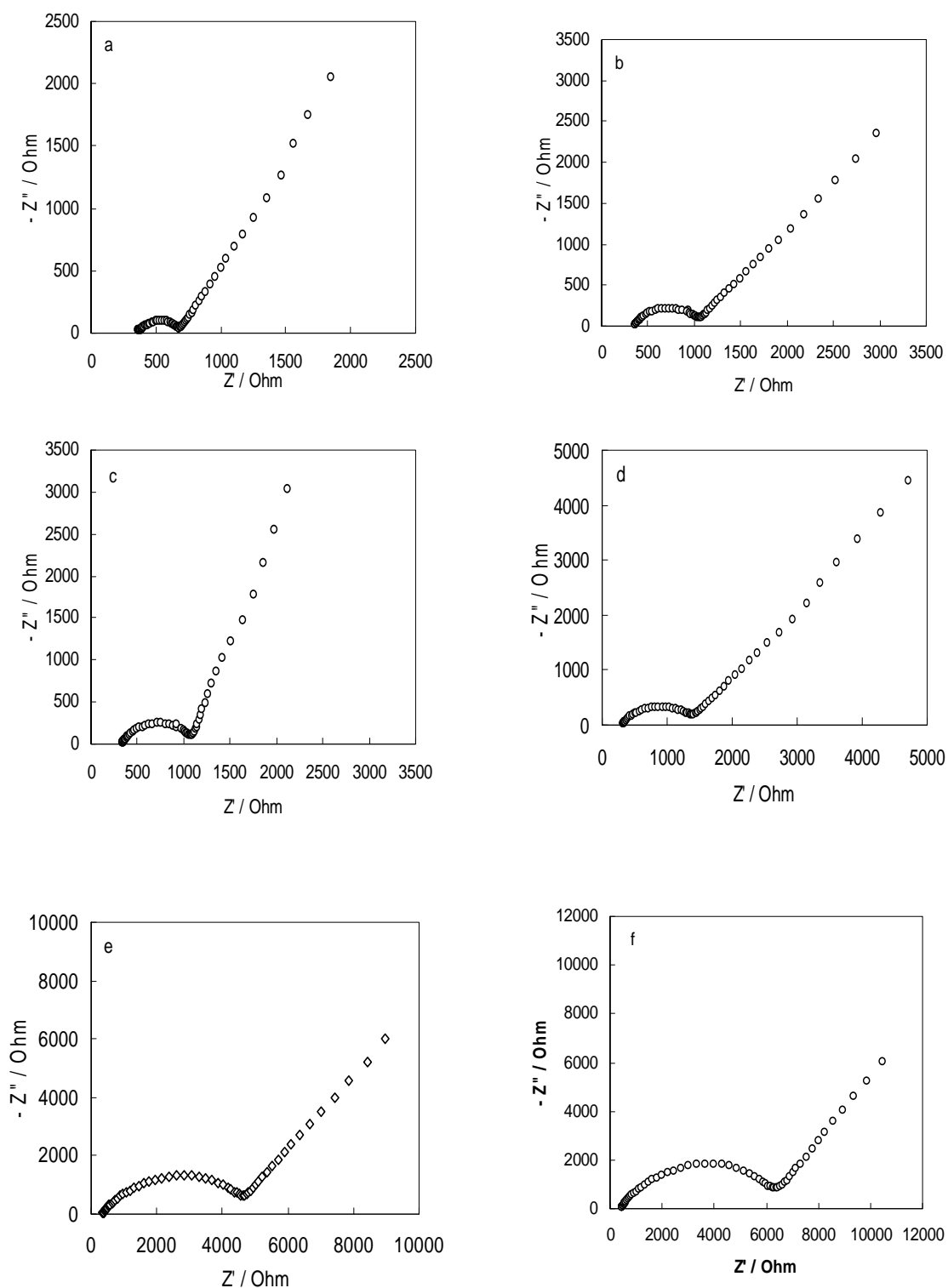


Figure 10. Ac impedance of Li/GPE/Li₂Pc cell after Charging to 4.2 V during (a)-(f): first – sixth charge- discharge cycle.

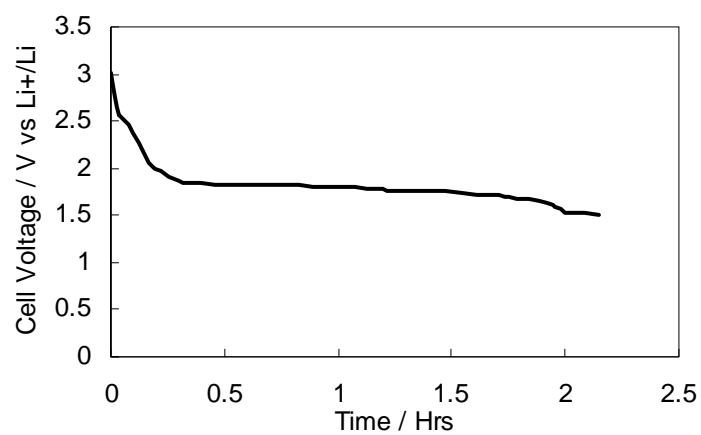


Figure 11. Discharge curve of a Li/GPE/Li₂Pc cell

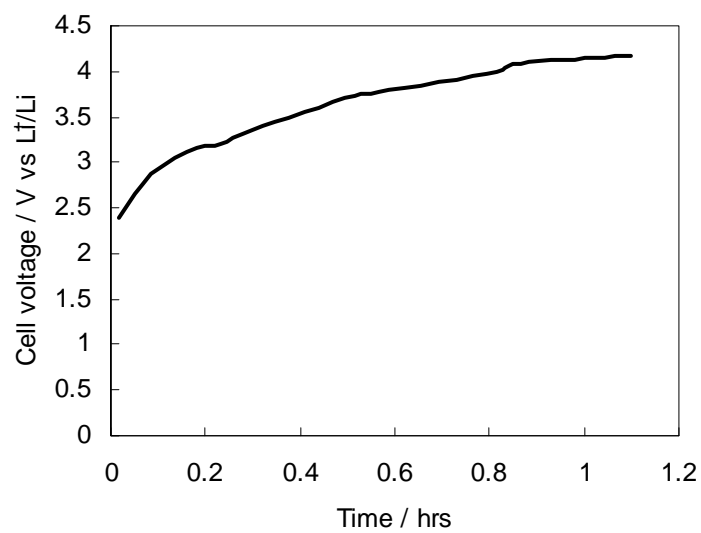


Figure 12. Charging curve of a Li/GPE/Li₂Pc cell

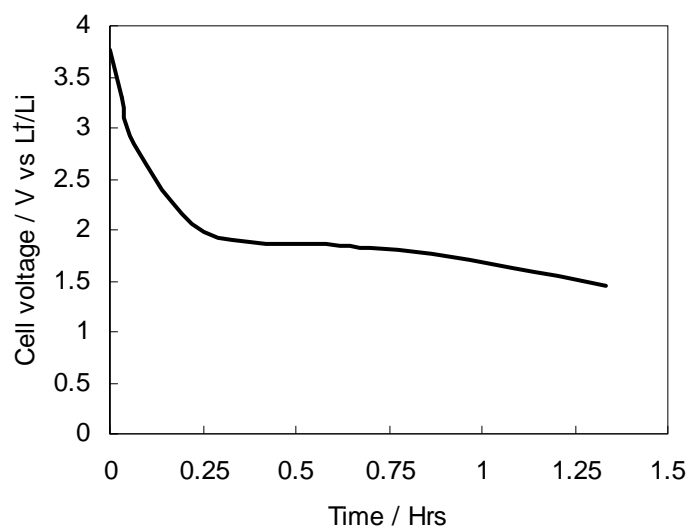


Figure 13. Discharge curve during 2nd cycle

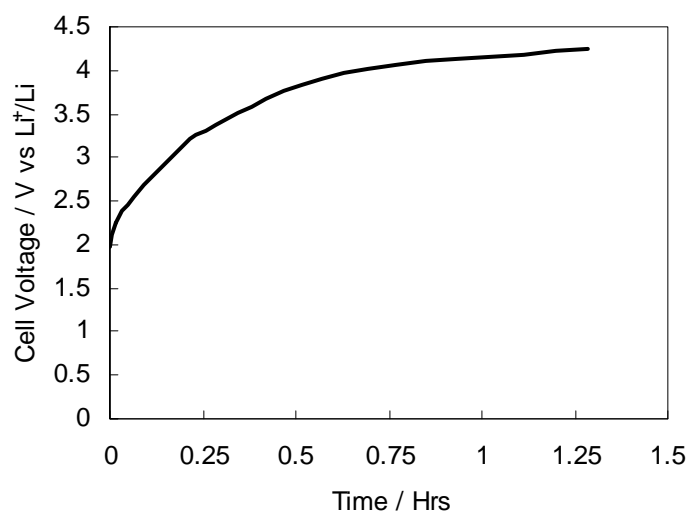


Figure 14. Charging curve during 2nd cycle

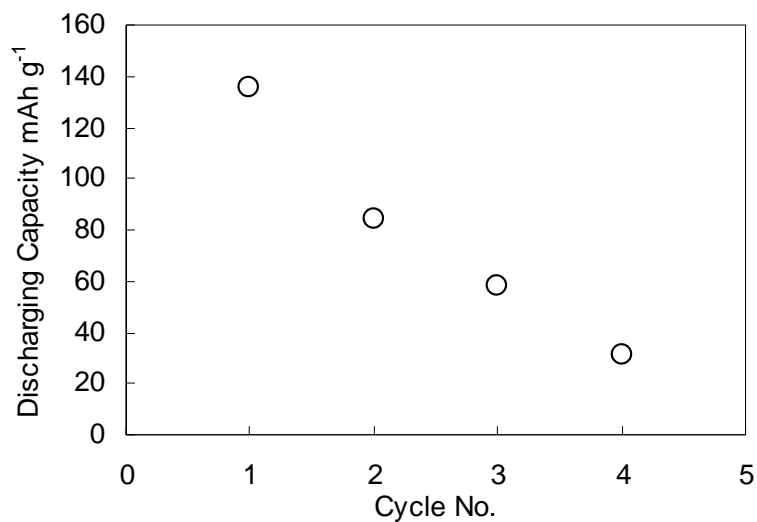


Figure 15. Variation of capacity with cycle number

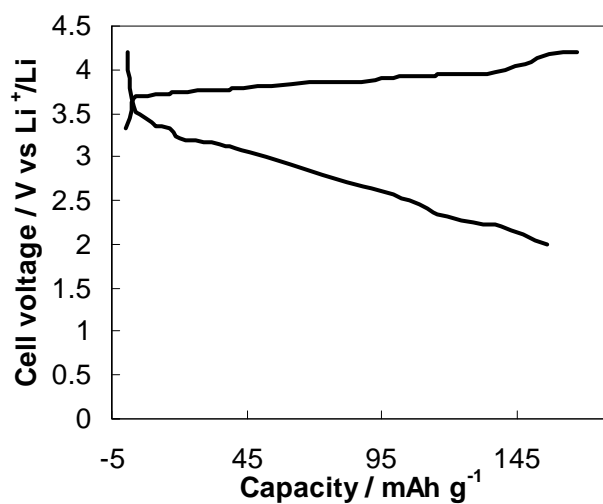


Figure 16. Charge-discharge curves of a Li/GPE/Li₂Pc cell

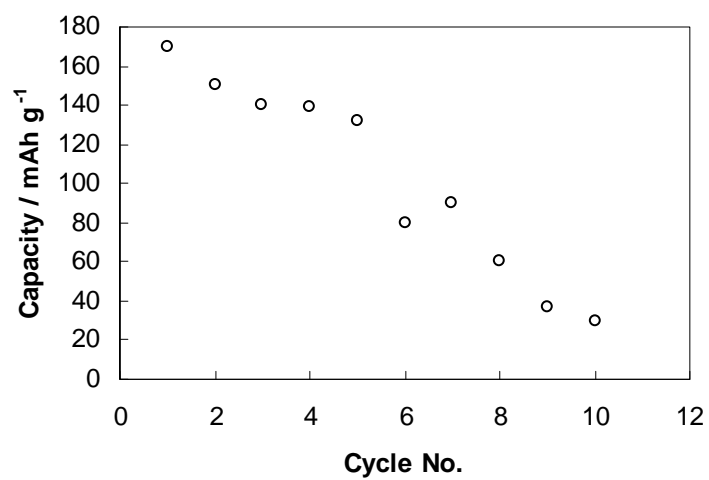


Figure 17. Cycle-life data of a Li/GPE/Li₂Pc cell.

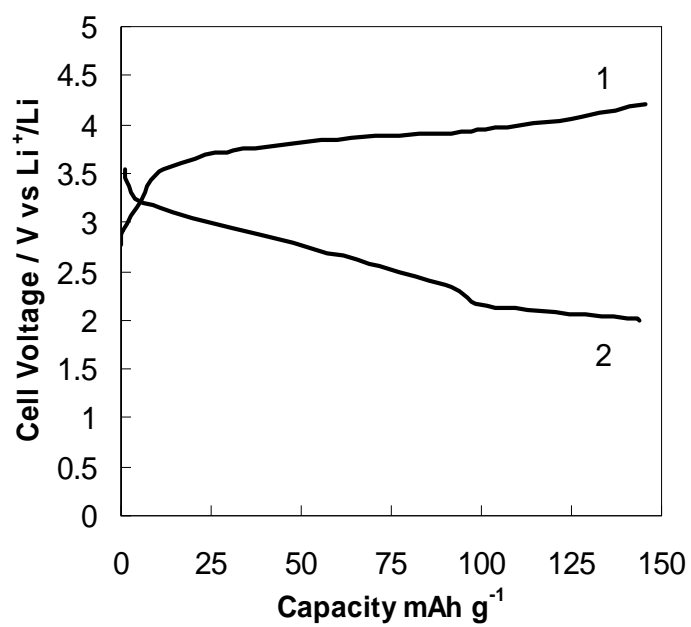


Figure 18. Charge-discharge curves of a Li/GPE/Li₂Pc cell.

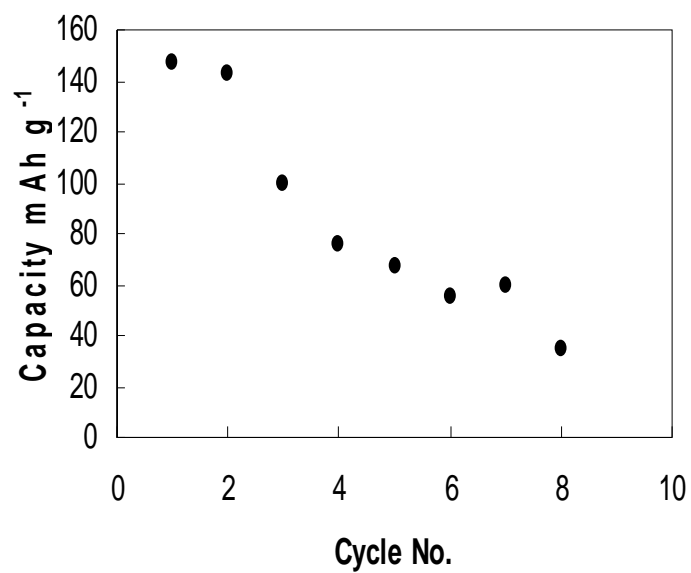


Figure 19. Cycle-life data.

LIST OF PUBLICATIONS

1. N. Munichandraiah, Rashmi and L.G. Scanlon
Electrochemical impedance studies of dilithium phthalocyanine.
Electrochemical Society Meeting, Honolulu, Hawaii, October 2004.
2. N. Munichandraiah , K. Sakthivel and L.G. Scanlon
Analysis of electrochemical impedance of dilithium phthalocyanine.
Electrochem. Solid State Lett. 8 (2005) E45 – E48.
3. K. Sakthivel, N. Munichandraiah and L.G. Scanlon
Electrodeposition of adherent films of lithium phthalocyanine on platinum and stainless steel substrates by oxidation of dilithium phthalocyanine.
J. Electrochem. Soc. 152 (2005) C756 – C763.

ACKNOWLEDGEMENTS

Author of this report extends his deep sense of gratitude to Dr. Lawrence G. Scanlon, AFRL, WPAFB for his constant support, encouragement and discussions. Without his interest and support, these studies could not have been possible. He thanks the officials of AOARD, Japan, who have been involved in monitoring this research contract for their constant administrative support and timely help.

Several Project Assistants have contributed to the studies of the research contract. All of them, in particular Mr. Sakthivel, are thanked for their sincere and hard work. Officials of Indian Institute of Science are thanked for their administrative support.